Geologia Croatica
Journal of the Croatian Geological Survey and the Croatian Geological Society
2025 | 78/3 | xxx–xxx | 12 Figs. | 9 Tabs. | www.geologia-croatica.hr

Deciphering the pedo-sedimentary complex of the eastern Adriatic coast: A case study from Privlaka, Croatia

Stanko Ružičić[1], Lidija Galović[2], Koen Beerten[3], Nina Hećej[2,4], Jasmina Martinčević Lazar[2], Rodoljub Gajić[5], Stjepan Husnjak[6], Rosa Maria Poch[7], Mihajlo Pandurov[5], Petar Stejić[5], Ajka Pjanić[2,*]

[1] University of Zagreb Faculty of Mining, Geology and Petroleum Engineering, Croatia
[2] Croatian Geological Survey, Zagreb, Croatia; (*corresponding author: apjanic@hgi-cgs.hr)
[3] Belgian Nuclear Research Centre SCK CEN, Mol, Belgium
[4] University of Bergen, Department of Earth Science, Bergen, Norway
[5] Geological Survey of Serbia, Belgrade, Serbia
[6] University of Zagreb, Faculty of Agriculture, Croatia
[7] Departament de Química, Física y Ciències Ambientals y del Sòl, Universitat de Lleida, Catalonia, Spain

doi: 10.4154/gc.2025.14

Article history:
Manuscript received: March 10, 2025
Revised manuscript accepted: July 8, 2025
Available online: September 25, 2025

Abstract

This study provides the first analysis of the Quaternary pedo-sedimentary complex to understand the succession of palaeosol and sediments, the mechanism of deposition, and the source and age of the material. Each distinctive layer was sampled. Palaeosols are rich in fine-grained components, predominantly silt. Quartz dominates in the light mineral fraction, suggesting that the sediments underwent more redeposition than for typical continental loess. The increase in weathered quartz grains with increasing depth could indicate that the proportion of fluvial sediments has increased compared to the aeolian sediments. Mineralogical and petrographic analyses confirmed the presence of chromite, serpentinite, and serpentinized olivine basalt, indicating an area of origin with ultramafic rocks, which could be the Dinaric ophiolitic zone in the hinterland. The carbonates are polygenetic in origin and consist of equal parts of highly spherical upper Cretaceous rudist limestones, Eocene nummulitic limestones, and low spherical pedogenic carbonate concretions, indicating local transport. According to the OSL dating results, the glacio-fluvial material is either early Weichselian or Saalian in age, while the palaeosol most likely cannot be younger than the Eemian and may even have a Middle Pleistocene age.

Keywords: palaeosol, sediment, glacio-fluvial transport, Dinaric ophiolitic zone, Quaternary, OSL

1. INTRODUCTION

Pedo-sedimentary successions refer to the vertical sequences of sedimentary deposits and associated palaeosol horizons that have been altered by pedogenic processes (RETALLACK, 2019). These successions result from the interaction between sedimentation and soil development over time. The study of pedo-sedimentary successions is widely used to obtain information on various aspects of Earth history (RETALLACK, 2019), e.g., palaeoenvironmental and geomorphological changes, material transport and palaeoclimatic interpretations and reconstructions (DURN, 1996; CORREGGIARI et al., 1996; DURN et al., 1999, 2018a, 2021; SIART et al., 2010; WACHA & FRECHEN, 2011; GALOVIĆ, 2014; ÚJVÁRI et al., 2016; ZERBONI et al., 2015; SPRAFKE et al., 2020; MOLNÁR et al., 2021; PFAFFNER et al., 2024; BEERTEN et al., 2025, in press). When studying the loess-palaeosol sequence of Susak Island, WACHA et al. (2011) found that the northern Adriatic region represents a distinct and unique periglacial environment and should not be neglected in the study of global glacial-interglacial evolution. ZERBONI et al. (2015) investigated the effects of soil formation processes under different environmental conditions and found that the different stages of pedogenesis can be linked to the overall progressive cooling during the last glacial cycle. DURN et al. (2018b) investigated the polygenetic soils that formed on the loess accumulated during the Late Glacial. The authors found that the studied polygenetic profile on Susak Island developed from the Late Glacial to the Holocene through both normal pedogenesis and erosion/sedimentation-induced pedogenesis. Recently, BANAK et al. (2021) investigated the understanding of depositional mechanisms and palaeoclimatic conditions during the Pleistocene in the central part of the eastern Adriatic coast. The authors identified and described three different facies that formed during colder and warmer climatic conditions. They concluded that the siliciclastic material most likely originated from the Eocene sandstones of the flysch basins in Dalmatia, which were transported by wind and currents.

GALOVIĆ et al. (2023) investigated sands and intraformational palaeosol in the continental part of Croatia. The authors identified a previously unrecognized regional climatic period that interrupted the aeolian deposition. In addition, MOLNÁR et al. (2021) carried out a sedimentological reconstruction of two eastern Croatian loess-palaeosol sequences (Zmajevac and Šarengrad II) located on the right bank of the Danube River. In Zmajevac, the sedimentological data indicated the increased proportion of sand in the sampled partial sequences, which could indicate a higher wind speed during accumulation. GALOVIĆ et al. (2011) investigated the geochemical com-

position and magnetic susceptibility (MS) to correlate these parameters with the sedimentological data of the Upper Pleistocene loess/palaeosol sedimentary succession in Šarengrad, Croatia. The authors concluded that the correlation between geochemical composition and magnetic susceptibility is primarily a function of pedogenesis. In addition, BANAK et al. (2013) investigated loess/palaeosol profiles in Baranja. The authors found that, with few exceptions, the loess from Baranja is very similar to loess deposits from other Pannonian regions.

The subject of this study is the pedo-sedimentary succession of Privlaka (eastern Adriatic coast, Croatia), which represents a promising archive for paleoenvironmental changes, as it shows a clear alternation of palaeosol and (glacio-) fluvial deposits. The aim of this study is to describe the palaeosol and sediments and to define the area of origin for the development of the Privlaka pedo-sedimentary succession. To achieve this goal, mineralogical, sedimentological and physico-chemical analyses were carried out. In addition, the age of the complex is determined using optically stimulated luminescence (OSL) dating.

1.1. Study area

The wider research area (Fig. 1) consists of Upper Cretaceous deposits (K22 and K23), rudist limestones of the Turonian and Senonian periods, which formed in a quiet littoral to neritic environment (MAJCEN et al., 1970; MAJCEN & KOROLIJA, 1973; BANAK et al., 2021). The carbonate and clastic deposits from the Eocene (E12 and E23) transgressively overlie the deposits mentioned above. The lower Eocene is represented by highly fossiliferous foraminiferal limestones formed in a littoral environment (MAJCEN et al., 1970; MAJCEN & KOROLIJA, 1973; ILIJANIĆ et al., 2018). The clastic deposits of the middle and upper Eocene comprise the complex of deposits that continuously overlie the foraminiferal limestones. They consist of alternating marl and sandstone, and in the upper parts, conglomerates. This is the youngest preserved member of the continuous succession of Palaeogene deposits, which are covered by Quaternary deposits. The Quaternary deposits of the studied area are represented by Upper Pleistocene deposits: sands, sandy clays (Q13) and terra rossa (ts) (Fig. 1).

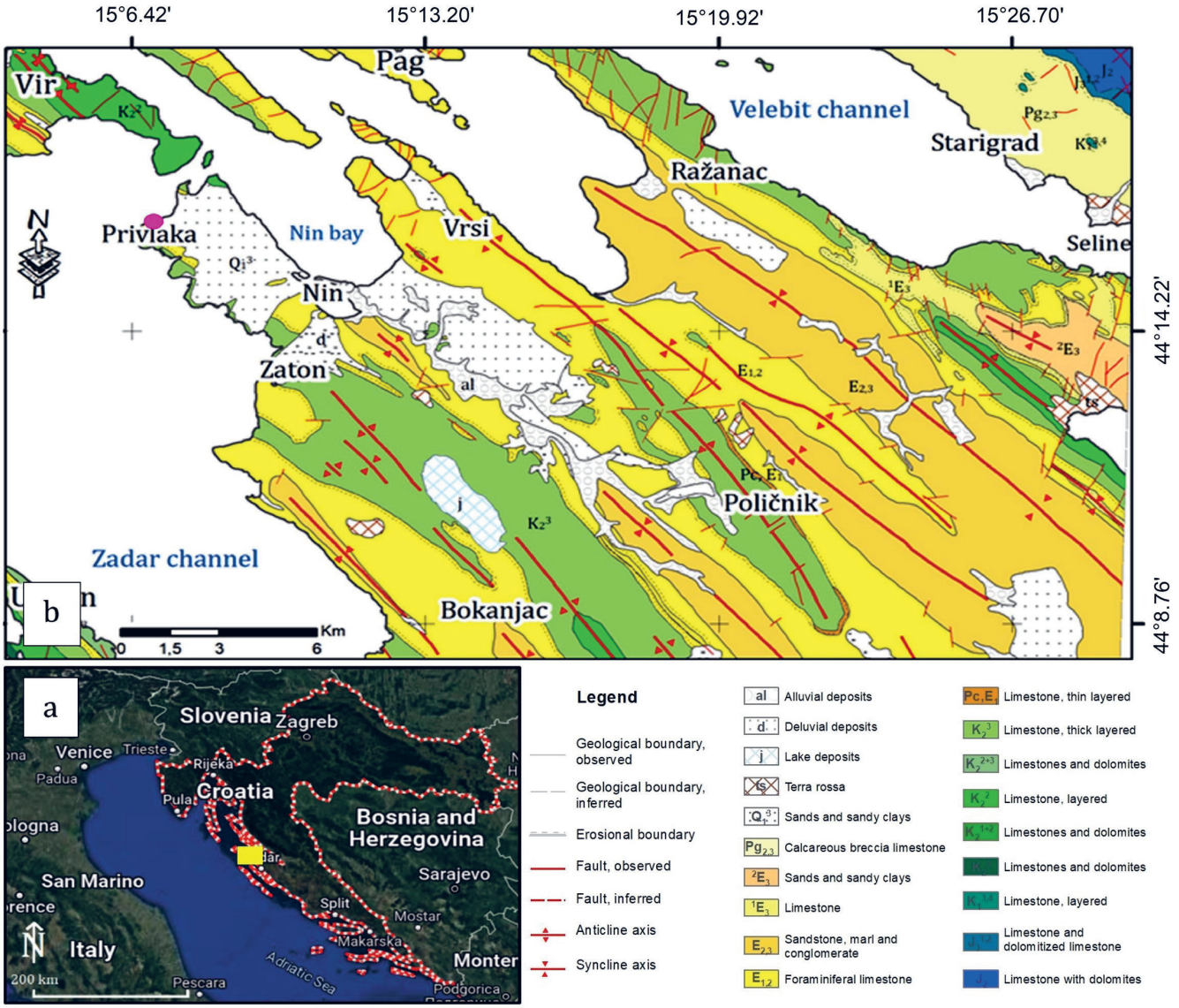

Figure 1. Location of the Privlaka pedo-sedimentary succession. **a** Geographical setting of the investigated succession (GOOGLE MAPS, 2025); **b** The geological setting of the wider Privlaka area (modified after MAJCEN et al., 1970; MAJCEN & KOROLIJA, 1973). The location of the investigated profiles is marked with a pink circle.

The composition of the deposits is determined by the palaeorelief of the underlying deposits and by the uneven dynamics of the depositional environment. Various factors, such as wind, seepage water, or hydrodynamic conditions in partially enclosed or occasionally flooded waters, could have been involved in the formation of such deposits. Such variable dynamics of the depositional environment can also be associated with changing climatic conditions. Intense relief erosion is correlated to the glacial period, while carbonate concretions are related to dry and semi-arid climates (MAJCEN & KOROLIJA, 1973). The youngest Quaternary deposits are represented by lakes and ponds (j), diluvial (d), and alluvial (al) deposits.

2. MATERIALS AND METHODS

2.1. Fieldwork

The Privlaka pedo-sedimentary complex (44° 15.98062' N, 15° 7.2409' E, WGS 84) is located about one kilometre northwest of the center of Privlaka. The complex has a total thickness of eight metres, but the upper two metres were not accessible. A field investigation was carried out in 2022. The field campaign began with the mechanical opening of a 0.5 to 1 m deep trench (PN1-5) in a six metre long profile within a pedo-sedimentary complex (Fig. 2). The six metre long succession of profile PN1-5 was described in sedimentological and pedological detail. In order to carry out a high-resolution investigation of the succession, the profile was sampled up to six metres for sedimentological and mineralogical analyzes.

2.2. Laboratory analyses

2.2.1. Grain size and morphological analysis of the grains

Particle size analysis was performed on 21 samples in the Croatian Geological Survey (HGI-CGS) laboratory using the sieving and pipette methods. The shape of the grains (sphericity and roundness) was analyzed for the fractions 1 – 0.5, 0.5 – 0.25, 0.25 – 0.125, 0.125 – 0.09, and 0.09 – 0.045 mm to reconstruct their transport history. Sphericity and roundness were estimated using the graphical table of KRUMBEIN & SLOSS (1963).

2.2.2. Physico-chemical properties

The carbonate content was determined for 13 samples using the SCM1 calcimeter (BEHR LABOR-TECHNIK, 2017) according to Scheibler's method. The carbonates were dissolved using hydrochloric acid (c(HCl) = 4 mol/l). The method was calibrated with pure $CaCO_3$. The pH value (H_2O) was determined according to HRN ISO 10390 (2005). The proportion of organic matter (%) was determined gravimetrically. Porcelain pots were annealed at a temperature of 450 °C, filled with

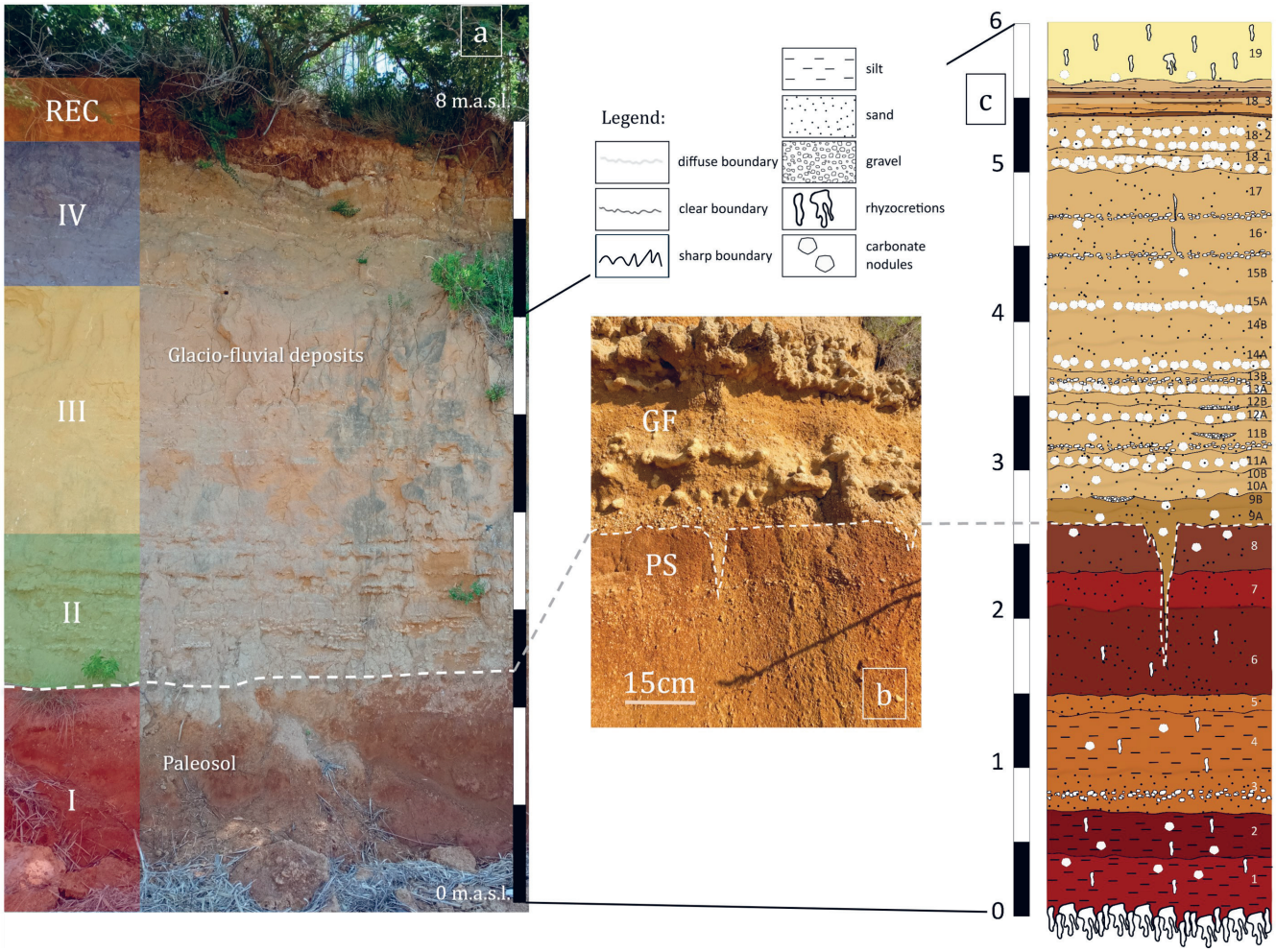

Figure 2. The pedo-sedimentary complex of Privlaka, profile **a** Units of the pedo-sedimentary complex; **b** Palaeosol(s) (PS)/glacio-fluvial (GF) erosion boundary with distinctive features; **c** Detailed graphical log of the profile PN1-5 with marked horizons/layers.

sample material weighing at least 0.5 g, and left in the oven at 110 °C overnight. The samples were then submerged in a 30% hydrogen peroxide solution in an amount sufficient to cover the entire sample. The sample was then annealed at 450 °C for 6 hours. The cooled samples were weighed, and the organic matter was calculated accordingly. The soil colour was determined in wet and dry conditions using the MUNSELL SOIL COLOUR CHARTS (2013).

2.2.3. Mineralogical properties

Mineralogical analysis using X-ray diffraction on powder samples was carried out in the HGI-CGS laboratory. Qualitative and semi-quantitative mineralogical analyzes were carried out on a total of 13 bulk samples using a PANalytical X'Pert powder X-ray diffractometer. The radiation source of the device is a copper tube that emits CuKα radiation with a wavelength of λ=1.54 Å. The diffractometer is equipped with a vertical θ-θ goniometer, a sample holder, an optical module to control the incident and diffracted radiation, a monochromator and a PIXcel detector. The X-ray diffractometer is controlled by the "X'Pert Quantify" software, while the diffraction patterns were analyzed using the X'Pert HighScore Plus software package, which is linked to an ICCD database of all known mineral species (PDF-4/MINERALS, 2024). X-rays are generated at a voltage of 45 kV and a current of 40 mA.

Due to the higher proportion of carbonates in the samples and to obtain a clear diffraction pattern of them, the insoluble residue was also analyzed. The insoluble residue was obtained by dissolving the carbonates with a buffered solution (pH 5) of sodium acetate and acetic acid according to the procedure described in SHANG & ZELAZNY (2008).

Semi-quantitative mineralogical analysis of the bulk samples was performed using the Rietveld method, in which the standard mineral profiles identified in the sample are refined with the profile obtained from the recorded data. The interpretation of the diffraction patterns and the refinement process were carried out using the X'Pert HighScore Plus software package, which is linked to a database of all known minerals and their structural, chemical and crystallographic data required for semi-quantitative analysis. The accuracy of the obtained results may vary from the actual values within a range of ± 3 – 5%.

2.2.4. Modal analysis

To determine the qualitative and semi-quantitative mineral composition of heavy and light mineral assemblages, 21 samples from pedogenetic and glacio-fluvial horizons were analyzed.

After disaggregation in an ultrasonic bath and sieving to the size fraction 0.09 – 0.125 mm, the calcite was dissolved. This fraction was selected for analysis as it contains all virtual mineral types in a ratio representative of the bulk sample. The heavy mineral fraction (HMF) was separated using sodium polytungstate (SPT) (ρ = 2.8 g cm^{-3}). The slides of the heavy and light mineral fraction (LMF) were examined with the AxioLab.A1 polarizing microscope from Carl Zeiss. The qualitative and semi-quantitative composition of a sample was determined after identifying 300 – 400 grains and calculating the percentage of each mineral. Canada balsam was used as the embedding medium.

The weathering index (W.I.) was used to investigate the degree of alteration of the analyzed horizons. The W.I. was defined by BREWER (1976) and applied by FAIVRE et al. (2019) and GALOVIĆ et al. (2023) as the ratio of the proportions of resistant and non-resistant minerals: W.I. = (Zrn + Tur + Rt + Ttn + St + Grt) / (Ep-Zo + Amp + Px + Ky). Symbology is according to WARR (2021): Zrn – zircon, Tur – tourmaline, Rt – rutile, Ttn – titanite, St – staurolite, Grt – garnet, Ep-Zo – epidote-zoisite, Amp – amphibole, Px – pyroxene and Ky – kyanite. It is calculated on the basis of the four decimal places of the percentage contents of the analyzed minerals. A higher W.I. of a horizon indicates significant or repeated weathering of the analyzed grains due to prolonged exposure to a warm and humid geochemical environment (pedogenesis) and/or resedimentation.

2.2.5. Petrographic analyses

Determining the composition of gravels and coarser sands provides information about the mineral composition and the origin of the source material. In order to determine the age of carbonate grains, micropalaeontological analyses were carried out. Petrographic analyses were carried out at the Geological Institute of Serbia.

Thin-sections of sand grains were prepared and examined under the Carl Zeiss polarizing microscope, and petrographic and micropalaeontological analyses were carried out. In addition, 15 pebbles were macroscopically examined, which were embedded as an interlayer in the palaeosol horizon 3. The interlayer is 3 – 7 cm thick and extends over approx. 0.8 m.a.s.l. It is subhorizontal, slightly inclined towards the sea (approx. 12°) and slightly undulating. Pebbles with a 1 – 3 cm diameter were sampled along palaeosol horizon 3. Most of the pebbles were too small to make thin-sections, so they were analyzed using lenses and acids (standard methods of macroscopic petrography).

2.2.6. OSL dating

The samples for the determination of the equivalent dose (De) were taken by hammering light-tight cylinders into the profile. The samples were prepared according to the procedures described in BEERTEN et al. (2020, 2025). The quartz fraction between 90 – 250 μm was used for dating.

OSL measurements were performed with the Riso OSL/TL-DA-20 reader using blue LED stimulation and a Hoya U-340 UV filter to prevent stimulation light from reaching the photomultiplier tube. The measurements were done in the luminescence facility of the Belgian Nuclear Research Centre SCK CEN. Several aliquots (24) were prepared for each sample, using a 2 mm thick mask and silicone oil spray to attach the grains to stainless steel disks. Artificial doses were delivered using the built-in Sr-90 beta source operating at a dose rate of 111 mGy/s. Routine OSL measurements were performed by stimulating the sample for 40 s at 125 °C. OSL intensities were determined using the first 0.48 s of the signal and an early background subtraction (0.8 – 1.6 s). Three dose points were used for De-determination, with one recycling and one zero dose point.

Dose recovery and preheating plateau tests were performed to verify the performance of the applied single aliquot regeneration (SAR) protocol according to the recommendations of MURRAY & WINTLE (2003). In the dose recovery test, natural aliquots were bleached, and a known dose was given close to the expected dose measured by the SAR protocol. Four aliquots were used for each preheating temperature (10 s) in the range of 180 – 260 °C. These tests allowed us to select an appropriate preheat temperature of 240 °C (10 s) and a cut heat temperature of 200 °C. The subsequent dose recovery test resulted in a recovery rate of 0.98 ± 0.02. The relative standard deviation in the dose recovery test was 4.9%. For the De- calculation, aliquots were accepted if the values for recovery and recycling were <10 %.

Samples for the determination of dose rate (D) were taken after removing the OSL sampling cylinders from the profile by collecting sufficient sediment from the surrounding matrix (20 – 30 cm diameter from the sampling point). The dried sediment mass (105 °C) was then placed in tightly sealed plastic bottles (200 mL) and stored for three weeks. The samples were then measured using high-resolution gamma spectrometry. The activity concentrations were converted to radionuclide concentrations of the respective parent isotope (^{238}U, ^{235}U, ^{232}Th and ^{40}K), from which the dose rates were calculated using the conversion factors of ADAMIEC & AITKEN (1998). The dose rates were corrected for water content and beta dose attenuation (correction factor 0.9). Based on a qualitative assessment of the site history, the time-averaged water content was set to 10%, with a relative uncertainty of 0.5 times this value. The cosmic dose rates were calculated according to PRESCOTT & HUTTON (1994), and the internal alpha-radioactivity was considered (VANDENBERGHE et al., 2008).

3. RESULTS

3.1. Field description of pedo-sedimentary complex

The Privlaka pedo-sedimentary complex is located about one kilometre northwest of the center of the Privlaka settlement. As shown in Figure 2a, the 8 m thick succession is divided into five units. Nineteen horizons/layers were identified during the field investigations (Table 1). The first Unit (I) is divided into 8 horizons, the second (II) into 5 layers, each with two sub-

Table 1. Summary of the field description of the studied pedo-sedimentary succession.

Unites / Thickness (cm)	Layer / horizon	Sub-layers	Depths (cm a.s.l.)	Thickness (cm)	Color	Reaction with HCl	Reaction with H_2O_2
REC / ~ 40				Not sampled.			
IV / ~ 150				Not sampled.			
III / ~ 230	19	-	568-600	-	n.a.	2	n.a.
	18	18-3	528-568	40	10YR 4/6	2	0.5
		18-2	518-528	10	10YR 5/6	2	n.a.
		18-1	503-518	15	10YR 5/6	2	0.5
	17	-	470-503	33	10 YR 5/8	2	0.5
	16	-	446-470	24	10 YR 5/6	2	0.5
	15	15B	420-446	26	10 YR 5/8	2	0.5
		15A	407-420	13	10 YR 5/8	2	n.a.
	14	14B	385-407	22	10 YR 5/8	2	0.5
		14A	370-385	15	10 YR 6/6	2	0.5
II / ~ 120	13	13B	361-370	9	10 YR 6/6	2	0.5
		13A	354-361	7	10 YR 6/6	2	n.a.
	12	12B	350-354	4	10 YR 5/8	2	0.5
		12A	336-350	14	10 YR 6/6	2	n.a.
	11	11B	315-336	21	10 YR 5/6	2	0.5
		11A	304-315	11	10 YR 5/8	2	n.a.
	10	10B	295-304	9	10 YR 4/6	2	0.5
		10A	284-295	11	10 YR 5/6	2	n.a.
	9	9B	279-284	5	10 YR 6/6	2	0.5
		9A	269-279	10	10 YR 5/6	2	0.5
I / ~ 250	8	-	230-263	33	5YR 4/6	2	2
	7	-	208-230	22	5YR 5/6	2	2
	6	-	148-208	60	5YR 4/6	2	2
	5	-	138-148	10	7.5YR 5/6	2	2
	4	-	95-138	43	7.5YR 5/6	2	1
	3	-	72-95	23	7.5YR 5/6	2	1
	2	-	44-72	28	5YR 4/6	2	2
	1	-	0-44	44	5YR 5/6	2	2

Legend: 2 – bursting bubbles (evident dissolution); 1.5 – big bubbles; 1 – hearing, small bubbles; 0.5 – only hearing; n.a.– not analyzed

layers, and the third Unit (III) into 6 layers. The two lower layers of Unit III are divided into two sub-layers, and the upper layer consists of three sub-layers. The two upper units, four (IV) and recent soil (REC), were not accessible. A total of 21 samples were collected. Secondary carbonates, such as rhizoconcretions, pseudomycelium, carbonate nodules, carbonate concretions and scattered carbonate, were identified and classified following RETALLACK (2019) and POCH et al. (2024) and references within.

Unit I – palaeosol

The lowest package (Unit I, with a thickness of more than 250 cm) indicates the reddish palaeosol (Fig. 2a, b). At the bottom of Unit I is a sandy, loamy, slightly yellowish red (5YR 5/6) palaeosol soil horizon 1 with a thickness of about 44 cm (Fig. 2c; Table 1; MUNSELL SOIL COLOUR CHARTS, 2013). Vertically oriented carbonate concretions (rhizoconcretions) with a diameter of 8 – 12 cm are precipitated at a depth below 35 cm of horizon 1 (Fig. 2c). In addition to the concretions, an accumulation of carbonate nodules (gravel-sized) can be observed in the upper part of horizon 1. The second palaeosol horizon 2 of the investigated profile PN1-5 lies between 44 and 72 cm (Fig. 2c). It is a coarse-grained, sandy clay that is darker yellowish red (5YR 4/6) and has a thickness of 28 cm. Vertically oriented carbonate concretions 5 – 10 cm in diameter with rounded carbonate nodules are developed. In addition, this horizon shows a lot of carbonate coatings and scattered carbonate in the matrix of this horizon. The boundary with the lower horizon 1 is clear and undulating.

The next horizon 3 of the palaeosol part of the profile consists of 23 cm thick, strongly brown (7.5YR 5/6) loamy sand (Fig. 2c; Table 1). It consists of several thin gravel layers composed of igneous rock pebbles that are moderately and discontinuously cemented by carbonate minerals. The boundary with lower horizon 2 is gradual and undulating.

Horizon 4 of the palaeosol unit is between 95 and 138 cm (Fig. 2c; Table 1). It is a strong brown (7.5YR 5/6) clay loam with a thickness of 43 cm. There are accumulations of carbonate nodules, which are harder in the lower part (lower 10 cm) of the horizon. The carbonate nodules are sporadically rounded (up to 2 cm) or vertically oriented (Fig. 2c). The boundary to the lower horizon is distinct and undulating. Horizon 5 of the palaeosol consists of a 10 cm thick, strongly brown (7.5YR 5/6) clay loam. This horizon is dominated by gravel clasts (<6 mm) consisting of quartz and calcite. These rock fragments are covered with layers of clay, which can also be found on the walls of the root channels. The boundary to horizon 4 is undulating and sharply defined.

Horizon 6 of the palaeosol lies between 148 and 208 cm (Fig. 2c; Table 1). The soil texture of this horizon is sandy loam with a yellowish red colour (5YR 4/6). This horizon shows an accumulation of vertical carbonate nodules or rhizoconcretions. The boundary with the underlying horizon 5 is undulating and gradual.

Palaeosol horizon 7 consists of a 22 cm thick yellowish red (5YR 5/6) sandy loam with angular or subangular gravels (<6 mm). This horizon is characterized by carbonate coatings. The boundary to horizon 6 is undulating and clear. The uppermost palaeosol horizon 8 lies between 230 and 263 cm (Fig. 2c; Table 1). The soil texture of this horizon is clayey loam with a yellowish red colour (5YR 4/6). This horizon contains spherical, partially dissolved carbonate concretions and indeterminate infillings of the channels, such as wedges. The boundary with horizon 7 is undulating and sharp.

Unit II – glacio-fluvial material

Unit I is followed by the glacio-fluvial material of Unit II (Fig. 2a, b, c; Table 1), which consists of ca. 10 cm thick cyclic events (total thickness 120 cm), with grain size fining upward. The lower parts of the layers of Unit II consist of coarser-grained particles and carbonate nodules, partly cemented by calcium carbonate. In addition, several gravelly channel infillings and intercalations have been observed, along with imbrication of clasts were observed. The boundary between the palaeosol and the overlying sediment is abrupt, indicating erosion of the underlying sediment or palaeosol. The lowest layer 9 of Unit II (269 – 284 cm), which is divided into sublayers 9A and 9B, has a yellowish brown (10YR 5/6) to brownish yellow (10YR 6/6) colour (Fig. 2a, b, c; Table 1). This layer is silty to gravelly sand with carbonate and silicate components. This layer contains subangular carbonate pebbles with a maximum size of 6 cm.

The next layer above 10 (284 – 304 cm) with the sub-layers 10A and 10B consists of loamy to silty sand with sporadic clasts of partially cemented pebbles (approx. 1.5 cm). This layer has a yellowish brown (10YR 5/6) to dark yellowish-brown colour (10YR 4/6).

Layer 11 (sublayers 11A and 11B) consists of an 11 cm thick yellowish brown (10YR 5/8) loamy or silty sand with poorly sorted and partially cemented grains (Fig. 2b, c; Table 1). Spherical carbonate concretions with a diameter of 1 – 5 cm form up to 70% of this layer. Lens-like structures (30 cm wide and 3 cm deep) filled with gravel have developed in this layer. Layer 12 (336 – 354 cm) is divided into sublayers 12A and 12B and has a brownish-yellow (10YR 6/6) to yellowish-brown (10YR 5/8) colour (Fig. 2c; Table 1). This layer is a well-sorted silty to gravelly, partially cemented sand. The upper part of this layer contains spherical concretions (15 cm) occurring in smaller lenses. There are also spherical carbonate concretions with a diameter of approx. 4 cm.

Layer 13 (depth 354 – 370 cm, sub-layers 13A and 13B) has a brownish yellow colour (10YR 6/6). This layer is silty sand with gravel (the grain size fines upward from gravel to silty sand). Predominantly spherical carbonate concretions 7 cm in diameter are partially cemented and associated with fine-grained material. The coating of clasts was observed in these materials. The boundaries between sub-layers 13A and 13B are distinct and undulating.

Unit III – glacio-fluvial material

Unit II is continuously followed by Unit III with a thickness of about 230 cm. It appears that the material of Unit III is consistent with the material of Unit II, but shows differences in the duration of the cyclic events (the layers described are thicker in Unit III), but still shows a relative trend of fining upward, with obvious gravel intercalations (Fig. 2a, b, c; Table 1).

Layer 14 is divided into sub-layers 14A and 14B (370 – 407 cm) and consists of brownish-yellow (10YR 6/6), partially cemented, silty-gravelly sand. Predominantly hemispherical carbonate concretions with a diameter of 1.5 – 3 cm are observed. This layer shows an increasing refinement of the grain size upward.

Layer 15 (depth 407 – 446 cm, with sub-layers 15A and 15B) consists of yellowish-brown (10YR 5/8) well-sorted gravelly sand with silt. Spherical carbonate concretions 2.5 cm in diameter are observed. Pebbles fill subvertical cracks developed from roots. The boundary with the lower layer is diffuse and irregular.

Layer 16 consists of 24 cm thick yellowish-brown (10YR 5/6) silty sand with rare subrounded gravel clasts (Fig. 2c; Table 1). There are fining material upward cycles (from 12% gravel in the lower to 5% in the upper part of the horizon). Subvertical root channels with carbonate coatings appeared in this layer. These holes are the boundary to the lower layer which is diffuse and irregular. The next layer 17 consists of silty sand with rare pebbles (up to 4 mm) and has a yellowish-brown colour (10YR 5/8). Root holes with sporadically infilled fine-grained material are observed. The boundary with the lower layer is diffuse and irregular.

Layer 18 is developed between 503 and 568 cm and was divided into three sublayers 18-1, 18-2 and 18-3 based on the alteration of three sets of coarse-grained material with concretions (partial cemented) and fine-grained material (Fig. 2c; Table 1). The coarse-grained material is 8 cm thick and consists of gravelly silty sand. The fine-grained material has a thickness of 1.5 cm and consists of silty sand. The sub-layer 18-1 consists of 15 cm thick gravelly sand with clasts up to 5 mm. This sub-layer is partially cemented with silt. The mostly spherical carbonate concretions with a diameter of 1.5 – 2 cm are post-sedimentary connected with the silt. Traces of recent animal burrows were found in sub-layer 18-2. The gravelly to silty sand is incompletely cemented. Sub-layer 18-3 consists of 40 cm thick, silty sand. It is weakly lithified and cemented with silt. In some places, fine material is observed towards the top. The boundary with the upper layer 19 is diffuse and undulating and is defined by a difference in texture and orientation of the accumulated secondary carbonates.

Layer 19 (568 – 600 cm) is a very compact silty sand with gravel. Subvertically oriented concretions (rhizoconcretions) were observed.

Unit IV – glacio-fluvial material and Unit REC – recent soil

Unit IV was formed from glacio-fluvial material with a total thickness of ca. 150 cm (Fig. 2a; Table 1). There are cyclic events in which the grain size becomes finer towards the top. At the top of the pedo-sedimentary complex is the REC unit. It consists of about 40 cm of recent, intensively rooted, weak soil. Due to the very inaccessible, collapse-prone material, the two uppermost units of the pedo-sedimentary complex were not sampled.

3.2. Grain-size distribution

According to the grain size analysis, the sand fraction predominates in the upper part (GF), while silt predominates in the lower part (PS) of the profile (Fig. 3). Medium and fine sand grains seem to equally represent the sand fraction in the GF material. Therefore, most samples are classified as fine sand or, more rarely, medium sand (WENTWORTH, 1922). In the lower part of the profile (PS), the silt component predominates, although there are some parts with more than 20% sand content and less than 40% silt (Fig. 3). Most of the samples are medium to coarse silt (WENTWORTH, 1922). The clay con-

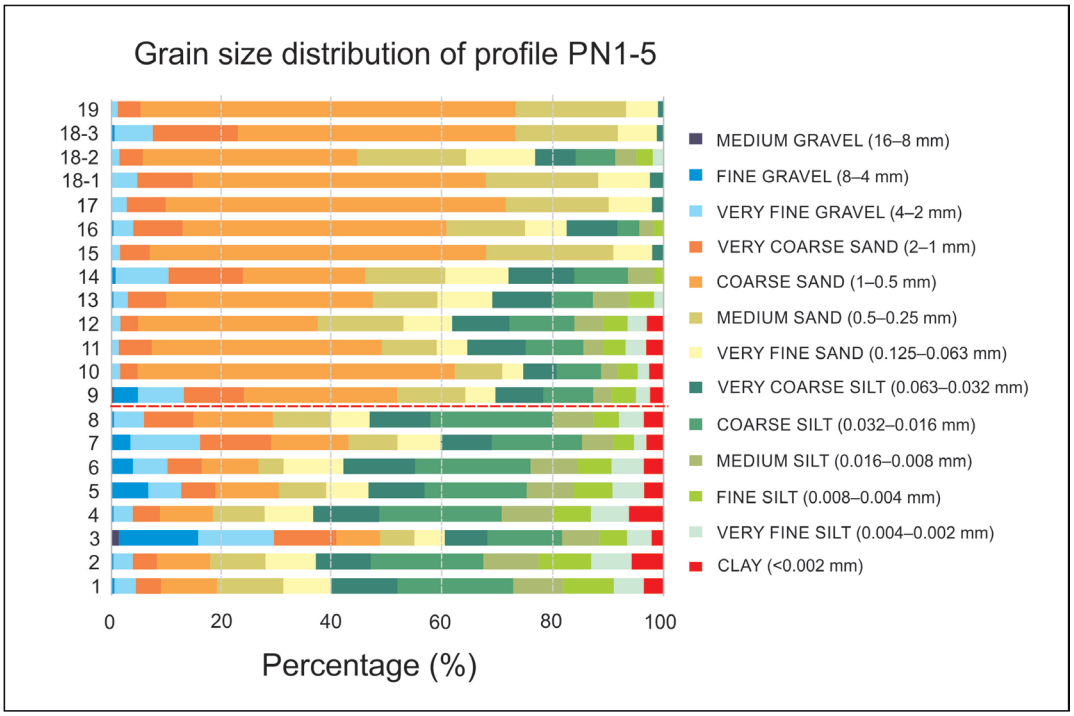

Figure 3. Grain size of the profile PN1-5. The red dashed subhorizontal line represents the border between Unit I – palaeosol(s) (PS) and Unit II – glacio-fluvial material (GF).

Table 2. Results of the morphologic analysis of the grains (KRUMBEIN & SLOSS, 1963).

Sample	Roundness					Description	Sphericity					Description
	Fraction (mm)						Fraction (mm)					
	1-0.5	0.5-0.25	0.25-0.125	0.125-0.09	0.09-0.045		1-0.5	0.5-0.25	0.25-0.125	0.125-0.09	0.09-0.045	
18-3	0.158	0.149	0.146	0.143	0.618	subangular	0.675	0.651	0.638	0.63	0.142	low sphericity
17	0.181	0.156	0.147	0.143		angular	0.678	0.648	0.626	0.611		moderate sphericity
13B	0.183	0.167	0.147	0.142		angular	0.678	0.655	0.635	0.626		moderate sphericity
9B	0.158	0.148	0.144	0.141		angular	0.66	0.645	0.631	0.618		moderate sphericity
9A	0.186	0.171	0.153	0.147		angular	0.655	0.633	0.615	0.596		moderate sphericity
8	0.172	0.156	0.147	0.143		angular	0.675	0.651	0.636	0.618		moderate sphericity
7	0.188	0.164	0.148	0.145		angular	0.685	0.655	0.64	0.626		moderate sphericity
6	0.17	0.157	0.148	0.145		angular	0.683	0.668	0.656	0.643		moderate sphericity
5	0.166	0.157	0.147	0.149		angular	0.686	0.663	0.645	0.631		moderate sphericity
4	0.168	0.157	0.149	0.145		angular	0.673	0.66	0.638	0.625		moderate sphericity
3	0.21	0.181	0.163	0.149		angular	0.581	0.58	0.568	0.56		low sphericity
2	0.189	0.172	0.162	0.153		angular	0.648	0.631	0.608	0.601		moderate sphericity
1	0.241	0.221	0.196	0.172		subangular	0.638	0.635	0.626	0.618		moderate sphericity

tent is higher in the palaeosol, where the pedogenetic processes were most intense.

There is no significant difference in the shape of the grains between the samples examined (Table 2). Both roundness (ranging between 0.14 and 0.62) and sphericity (ranging between 0.14 and 0.68) show a decreasing tendency with smaller grain sizes in most of the individual samples. Only two samples consist of subangular grains. One from palaeosol and the other from (glacio-) fluvial material. Almost all samples show a medium sphericity. Two samples (3 and 18-3) have low sphericity.

3.3. Physico-chemical properties

The results of the physico-chemical properties within the PN1-5 profile are shown in Figure 4. All analysed samples have an alkaline pH_{H2O} (>7.5). The percentage of organic matter (OM) is higher in the palaeosol part of the profile than in the glacio-fluvial part, which is due to pedogenetic development. The $CaCO_3$ content generally decreases with depth. In the upper part of the profile (glacio-fluvial sediments), this content varies between 60.8% and 86.7%, while in the lower part it is between 16.8% and 29.7%.

3.4. Mineralogical properties

The mineralogical composition (of the <2 mm fraction), indicates the predominant mineral phases identified by X-ray powder diffraction in the bulk sample, and is shown in Table 3. The predominant minerals in the palaeosol horizons in the lower part of profile PN1-5 are calcite and quartz. The samples also contain feldspars, goethite, phyllosilicates and sporadically titanium oxides (Table 3). Two types of calcites are distinguished in the palaeosol and glacio-fluvial sediments: primary calcite, which was formed by the process of physical weathering of carbonate rocks from the hinterland, and secondary, i.e., authigenic calcite, which was precipitated as cement in carbonate concretions and rhizoconcretions during pedogenesis.

Table 3. Semi-quantitative determination of mineral composition in paleosol and (glacio-)fluvial samples on the fraction <2 mm.

Sample	Mineral composition of fraction <2 mm						
	Qtz	Cal	K-Fs	Pl	Gt	TiOx	Phy
18-2	****	***		*		*	*
17	**	****	*	*			*
13B	**	****		*	~	*	*
9B	**	****					*
9A	**	****		*	*		
8	***	***	*	*	*	~	**
7	**	****		*	*	*	*
6	***	**	*	*	*		**
5	***	****		*	*		*
4	**	***	*	*	*	~	**
3	**	***		*	*	*	**
2	***	***	*	*	*		**
1	****	**	*	*	*		**

Legend: Qtz – quartz, Cal – calcite, Phy – phyllosilicates, K-Fs – potassium feldspar, Pl – plagioclase, Gt – goethite, TiOx – titanium oxides (rutil and anatas)
**** – predominant (> 50 w%), *** – dominant (35 – 50 w%), ** – abundant (15 – 35 w%), * – subordinate (1 – 15 w%), ~ in traces (< 1 w%).

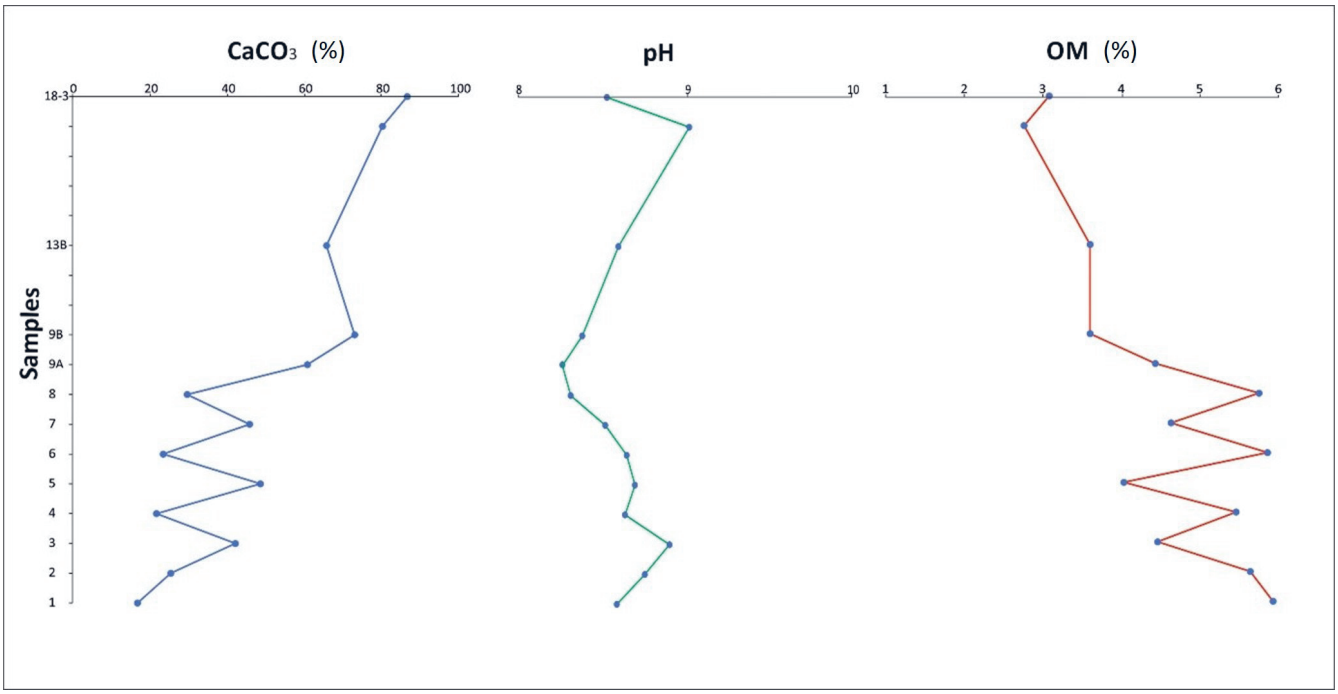

Figure 4. Distribution of the $CaCO_3$ (%), pH, and OM (%) along the PN1-5 profile.

After carbonate dissolution (Table 4) the visibility of titanium oxides increased. They are identified in nearly all insoluble residue samples, typically as subordinate components, and as traces in some samples. These results indicate that titanium oxides are a consistent but minor component of the mineral assemblage, the detectability of which increases after carbonate dissolution. In some horizons there is sporadic evidence of chromium hydroxides, manganese hydroxides and magnetite. However, this cannot be confirmed with certainty as the diffraction reflections of these minerals overlap with the diffraction reflections of some other mineral types.

Quartz is the dominant mineral in the insoluble residue of glacio-fluvial sediments. Other minerals identified in the insoluble residue are feldspars and goethite. Unlike goethite, the content of which is unchanged in both parts of the profile, the content of feldspar is somewhat more variable. Very broad and less intense diffraction reflections of 10 Å and 14 Å from clay minerals indicate their presence in the very small size fraction. They are more abundant in the palaeosol than in the GF sediments of the upper part of the profile. Their abundance also changes over the profile, which could be related to illuviation processes.

3.5. Modal analysis

The LMF is about 98% in almost all samples (Fig. 5; Table 5), with quartz being the dominant component (79 – 92%) (Table 6), followed by lithic particles (5 – 15%) and feldspars (3 – 7%). Volcanic glass is an accessory (<3 %). Fresh quartz

Table 4. Semi-quantitative determination of the mineral composition of insoluble residue.

Sample	Mineral composition of insoluble residue							
	Qtz	K-Fs	Pl	Gt	TiOx	Cr_{HOX}	Phy	Mg
18-2	****		*		*		**	
17	****	*	*	*			**	
13B	****	**		*	*		**	
9B	****	*	*	*	*		*	
9A	****	*	**	*	*		*	
8	***	**	*	*		?	***	
7	**	*	*	*			***	?
6	**	*	**	*	~		****	?
5	**	**			~	?	****	?
4	***	*	*	*	~		***	
3	***		**	*	*		***	
2	**	**	*	*	*		****	
1	**	*	*	*			****	

Legend: Qtz – quartz, K-Fs – potassium feldspar, Pl – plagioclase, Gt – goethite, TiOx – titanium oxides (rutil and anatase), Cr_{HOX} – chromium hydroxides, Phy – phyllosilicates, Mg – magnetite, ? – indication for the presence, ~ in traces (< 1 w%)

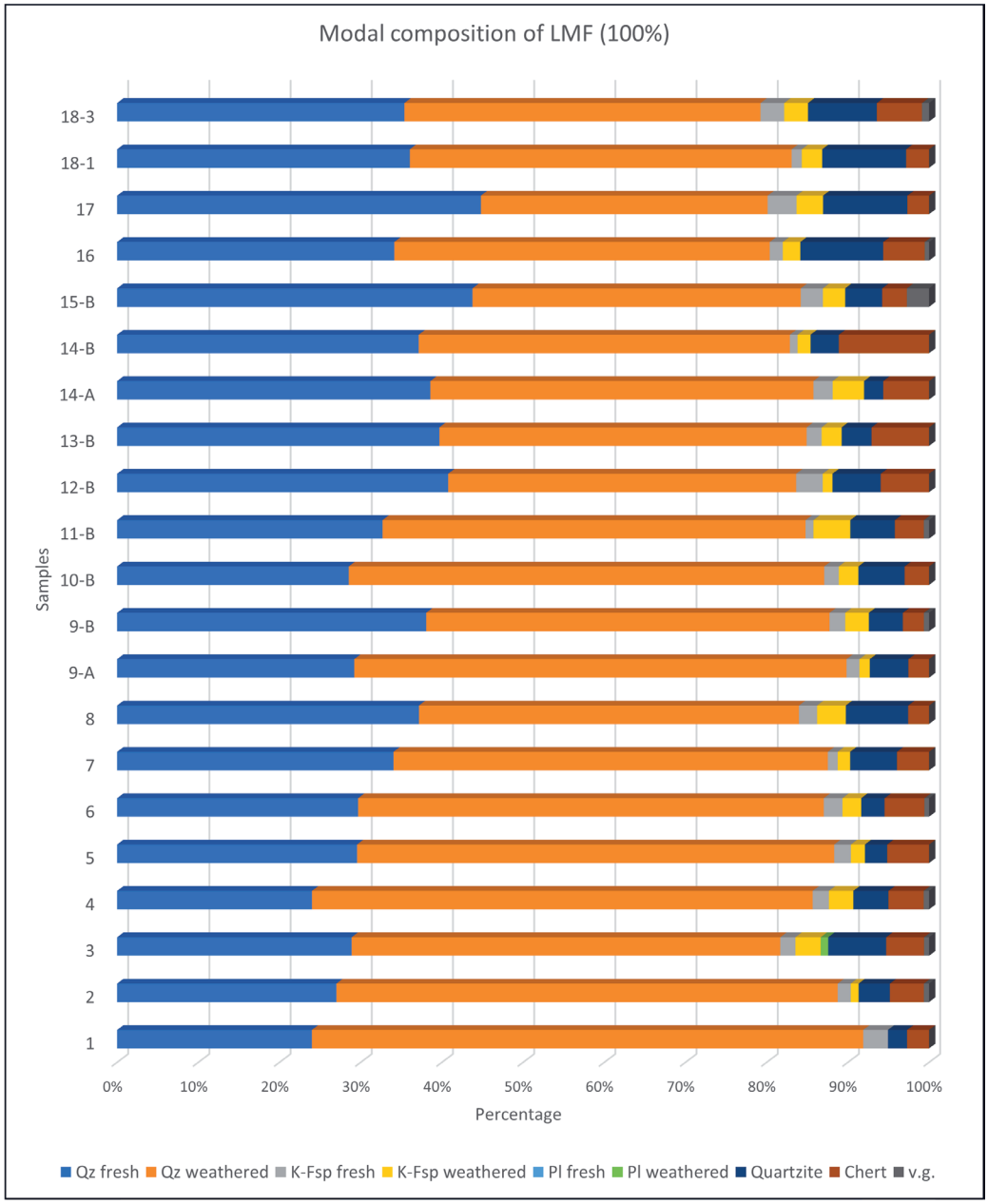

Figure 5. Modal composition of the LMF (values in %).

grains are often idiomorphic (Fig. 6a) with (zircon) inclusions. There is a general trend towards an increase in the proportion of weathered quartz grains compared to fresh ones (Fig. 6b), which increases with the age of the samples (Fig. 2). The ratio ranges from almost 3 in the oldest palaeosol to 1.5 and 2.5 in the overlying palaeosol horizons and the older glacio-fluvial sediments to about 1 (equal distribution of weathered and fresh grains) in the uppermost 2.5 m of the studied part of a profile PN1-5 (Fig. 2). This ratio is not reliable when applied to feldspars, as these are only minor contributors to the mineral assemblage (Tables 5 and 6). Plagioclase is rare; weathered K-feldspars are mostly represented by orthoclase, rarely by microcline. Weathered feldspars are kaolinized and sometimes even sericitized and contain no inclusions, while fresh feldspars are sanidine or adular. In rare cases, they contain inclusions that have been determined as idiomorphic zircon inclusions. Some fresh feldspar grains consist of hypidiomorphic sanidine (Fig. 6c). Lithic particles are represented by quartzite (2 – 10%), chert (3 – 11%) and rarely by volcanic glass (up to 1(3) %). Horizons 16 – 18-1 are enriched with quartzite, and horizon 14B with chert (Table 5). Some chert particles are siliceous spicules of fossil sponges exposing the internal axial channel (Fig. 6d) and the fossil zonal chert ball (Fig. 6e). Some cases may represent myrmekite intergrowths. The quartzite crystals are characterised by undulous extinction. Volcanic glass is sometimes clear with weak negative relief but usually devitrified and represented by spherulites of radial quartz fibres with extinction cross (N+). It may be a chalcedony with a "Maltese cross" (Fig. 6f). Volcanic glass with inclusions and devitrified volcanic glass is enriched in the 15B horizon. In addition to the reported lithic particles, serpentinite particles (specific density 2.6 g cm^{-1}) plastered with quartz grains are found in the oldest 18-1 horizons (Fig. 6g).

Table 5. Modal composition of light mineral fraction (values in %) and Weathering index (Legend in Table 6).

Sample	Depth from the surface (cm)	Quartz		Feldspar				Lithic particles			[2]W.I.
				K-feldspar		Plagioclase					
		fresh	weathered	fresh	weathered	fresh	weathered	quartzite	chert	[1]v.g.	
18-3	528–568	35	44	3	3	0	+	8	6	1	35
18-1	503–518	36	47	1	3	0	0	10	3	0	36
17	470–503	45	35	4	3	0	0	10	3	+	45
16	446–470	34	46	2	2	0	0	10	5	1	34
15 B	420–446	44	40	3	3	+	+	5	3	3	44
14 B	385–407	37	46	1	2	0	0	3	11	+	37
14 A	370–385	38	47	2	4	+	0	2	6	0	38
13 B	361–370	40	45	2	2	0	0	4	7	0	40
12 B	350–354	41	43	3	1	0	0	6	6	+	41
11 B	315–336	33	52	1	5	0	0	6	4	1	33
10 B	295–304	28	58	2	2	0	0	6	3	+	28
9 B	279–284	38	50	2	3	0	+	4	3	1	38
9A	269–279	29	60	2	1	0	0	5	3	+	29
8	230–263	37	47	2	4	+	0	8	3	0	37
7	208–230	34	53	1	2	0	0	6	4	+	34
6	148–208	30	57	2	2	0	+	3	5	1	30
5	138–148	29	59	2	2	0	+	3	5	0	29
4	95–138	24	61	2	3	0	+	4	4	1	24
3	72–95	29	53	2	3	0	1	7	5	1	29
2	44–72	27	62	2	1	0	0	4	4	1	27
1	0–44	24	68	3	0	0	0	2	3	0	24

[1]v.g. – volcanic glass; **[2]W.I.** – Weathering index; + – minerals with occurrence <0.5 %

Table 6. Modal composition of heavy and light mineral association.

Sample	Composition of LMF 100%				HMF %	Composition of HMF 100%					Transparent heavy minerals 100%									
	Qz	Fsp	L	v.g.		Op	Gth	Chl	Bt	THM	Ep-Zo	Amp	Px	Grt	Ky	St	Tur	Zrn	Rt	Ttn	Chr
18-3	79	6	14	1	1.87	54	18	+	0	27	5	2	5	43	0	1	5	13	14	1	10
18-1	83	4	13	0	2.33	57	13	1	0	30	7	1	8	46	2	2	9	14	6	1	5
17	80	7	13	+	2.51	30	30	+	+	40	6	2	6	37	0	1	6	20	12	4	6
16	80	4	15	1	2.31	36	22	0	0	42	7	1	4	46	0	1	4	18	13	1	5
15 B	84	6	8	3	2.16	36	21	0	0	44	7	2	9	29	1	1	3	18	17	5	8
14 B	83	3	15	+	1.82	38	26	0	0	37	8	2	10	27	3	4	7	15	19	1	3
14 A	86	7	8	0	1.68	44	18	0	0	38	3	1	9	40	0	2	13	14	14	3	1
13 B	85	4	11	0	1.94	36	17	+	0	46	7	0	5	51	1	2	5	12	13	0	5
12 B	83	4	12	+	1.31	31	26	0	+	43	4	2	7	28	1	4	4	20	21	4	5
11 B	85	6	9	1	1.76	36	33	1	+	31	5	4	5	39	0	4	9	11	15	3	6
10 B	87	4	9	+	1.24	36	29	0	1	34	9	4	13	31	0	3	11	14	9	2	5
9 B	87	5	7	1	1.88	47	24	0	0	29	5	6	8	34	2	4	13	8	11	4	4
9A	90	3	7	+	2.34	35	23	0	+	42	5	5	11	25	1	3	4	24	17	2	4
8	84	6	10	0	1.76	31	32	1	0	36	6	3	7	39	1	1	11	9	15	5	3
7	87	3	10	+	1.78	35	28	0	0	37	9	0	5	37	2	2	4	10	21	2	9
6	87	5	8	1	2.14	32	31	0	0	37	2	2	6	35	0	1	8	10	21	6	10
5	88	4	8	0	1.08	36	28	0	1	36	6	3	12	33	0	3	7	15	8	8	8
4	85	5	9	1	1.16	48	16	0	+	35	6	1	8	35	1	4	10	11	15	6	2
3	82	6	12	1	1.26	45	23	0	0	32	9	5	8	32	0	2	15	12	15	0	3
2	89	3	8	1	1.24	42	24	0	+	34	7	2	7	33	0	2	9	17	18	1	3
1	92	3	5	0	2.05	52	12	+	0	35	6	5	4	39	0	1	4	15	10	0	18

Legend: LMF – light mineral fraction, HMF – heavy mineral fraction, THM – transparent heavy minerals, Qz – quartz, Fsp – feldspar, L – transparent lithic particles, Op – opâque minerals, Gth – goethite, Chl – chlorite, Bt – biotite, Ms – muscovite, Ep-Zo – epidote-zoisite, Amp – amphibole, Px – pyroxene, Grt – garnet, Ky – kyanite, St – staurolite, Tur – tourmaline, Zrn – zircon, Rt – rutile, Ttn – titanite, Chr – chromite, Ap – apatite, v.g. – volcanic glass, + – minerals with occurrence <0.5 % (Symbology according to WARR 2021).

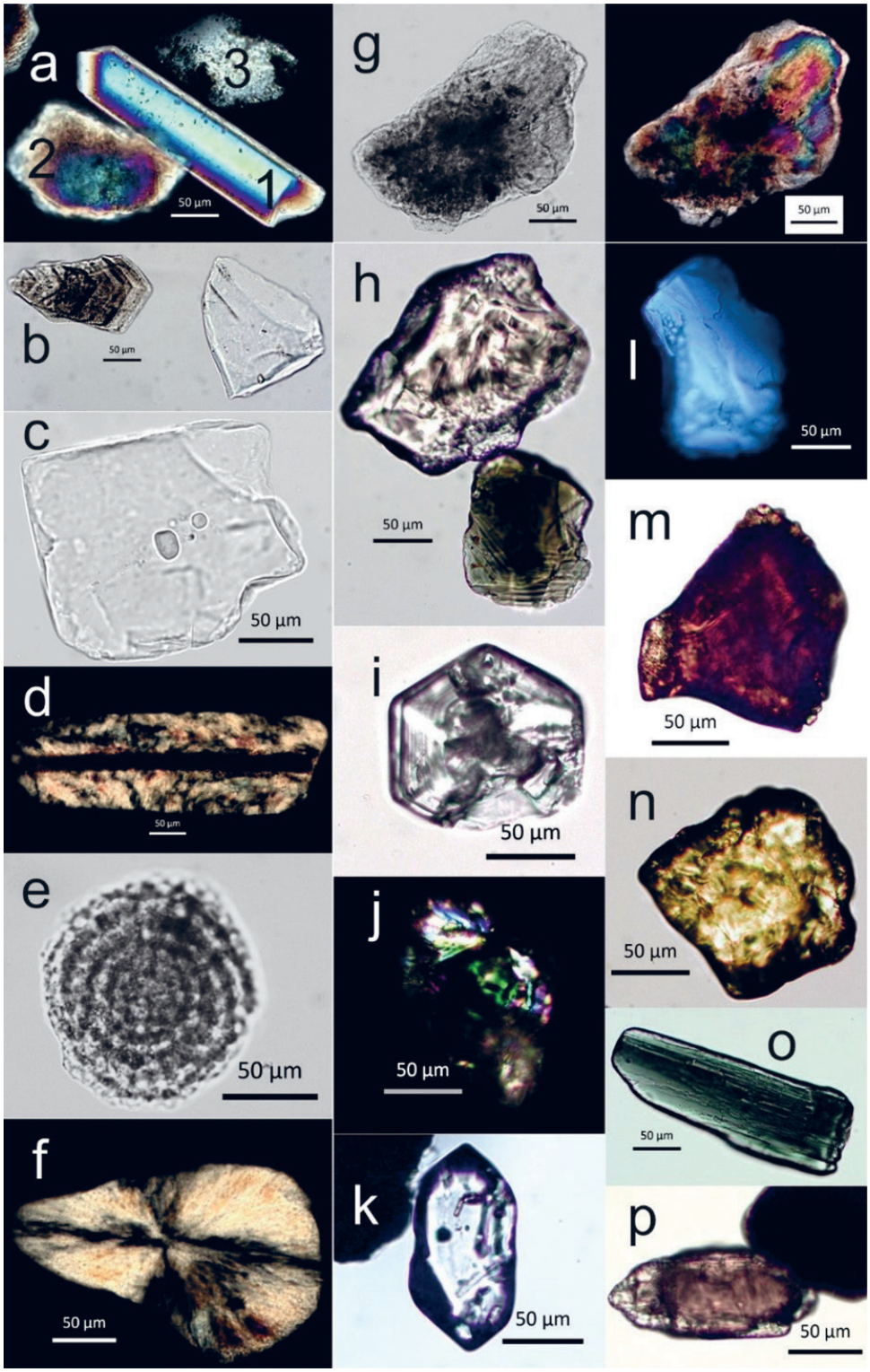

Figure 6. Photo-micrographs of minerals from the LMF and HMF of samples of the investigated PN 1-5 profile in parallel (N-) or crossed (N+) nicols: **a** Quartz fresh idiomorphic with inclusions (1), weathered (2) and with regeneration edge (3), N+, 7; **b** Weathered and fresh quartz, N-, 2; **c** Fresh hypidiomorphic sanidine with inclusions, N-, 3; **d** Siliceous spicule of fossil sponge with the internal axial channel, N+, 6; **e** Fossil zonal chert ball, N-, 10B; **f** Spherulites of radial fibres of quartz with extinction cross, N+, 3; **g** Serpentinite, N- and N+, 1; **h** Rounded, allotriomorphic and weathered garnet and tourmaline, N-, 1; **i** Fresh idiomorphic zonal garnet, N-, 9B; **j** Rounded zircon, N+, 1; **k** Idiomorphic zircon, N-, 9A; **l** Fresh zoisite with anomalous blue interference colour, N-, 11B; **m** Chromite, N-, 1; **n** Yellowish Cr-rich spinel (picotite?), N-, 1; **o** Fresh hornblende, N-, 12B; **p** Glaucophane, N-, 14B.

The distribution of the HMF is mostly uniform across the PN1-5 profile and lies between 1.08% and 2.51% (Fig. 7; Table 5). Opaque grains predominate among the HMF. In addition to indeterminate opaque grains (30 – 57% of the sample), there are also goethite grains (12 – 33%). When viewed under higher illumination, goethite microcrystals appear reddish in crossed nicols, whereas in parallel nicols they appear opaque due to their red microcrystals. They are alteration products of mafic minerals and often coat grains. The goethite grains are also roundish and have a high sphericity. Due to their uniqueness,

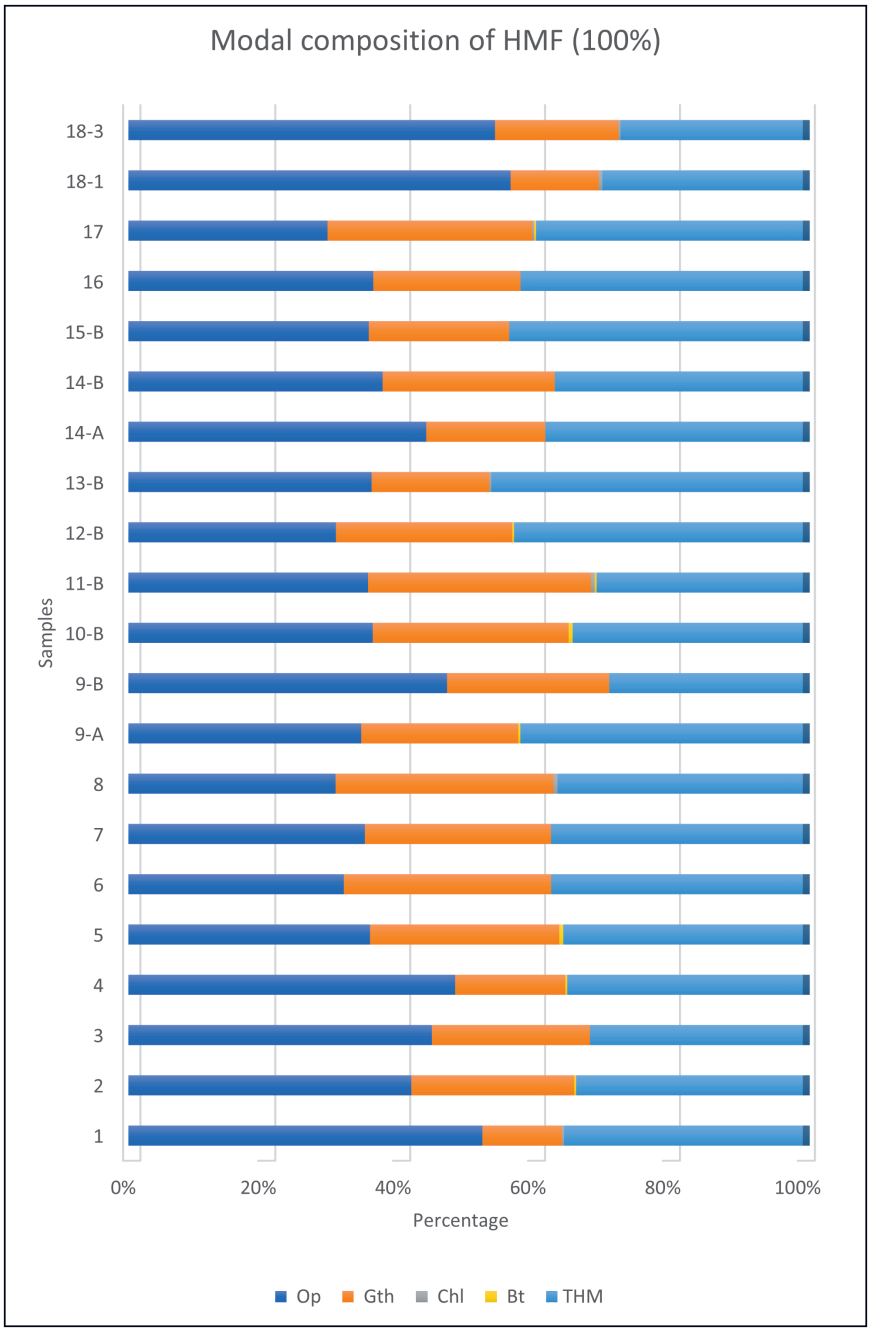

Figure 7. Modal composition of the HMF (values in %) (Legend in Table 5).

they are separated from the opaque grains, although they are part of them. The flaky minerals chlorite and biotite are rare (<1%), and muscovite is not present (except for some sericite grains). The proportion of transparent heavy minerals (THM) is 27 – 46% and shows no specific distribution trend (Fig. 8; Table 6). The most common transparent heavy minerals are resistant grains such as garnet (27 – 51%), followed by zircon (9 – 24%) and rutile (6 – 21%). Garnet grains can be brownish, pinkish or yellowish (Fig. 6h), but are usually colourless and rarely idiomorphic (Fig. 6i). Zircon crystals are usually (sometimes completely) rounded (Fig. 6j), but idiomorphic crystals are not uncommon (Fig. 6k). Smaller amounts of tourmaline (3 – 15%), pyroxenes (4 – 13%) and chromite (1 – 18%) are present. Tourmaline crystals are often roundish, allotriomorphic and weathered (Fig. 6h), rarely idiomorphic and hypidiomorphic crystals. The pleochroic colours are olive green, black and colourless to yellowish. It is partially enriched in the palaeosol. In horizon 11B, all tourmaline crystals are regularly allotriomorphic. The pyroxenes are mostly orthopyroxene, which is rarely fresh and is clearly enriched in the oldest horizon 6. The epidote-zoisite group (2 – 9%), titanite (<8 %), amphibole (<6 %), staurolite (1 – 4%) and kyanite (<2 %) only occur sporadically. The epidote-zoisite group is predominantly represented by zoisite, which has an anomalous blue interference colour. Fresh grains are more common in samples 10B and 11B (Fig. 6l). In addition to chromite as Cr-rich reddish spinel (Fig. 6m), this category also includes spinels of other colours, such as yellowish-brown Cr-rich spinel (picotite?), which is characteristic of basic and ultrabasic rocks and is associated with volcanic rocks, peridotites and serpentinites (Fig. 6n). Amphi-

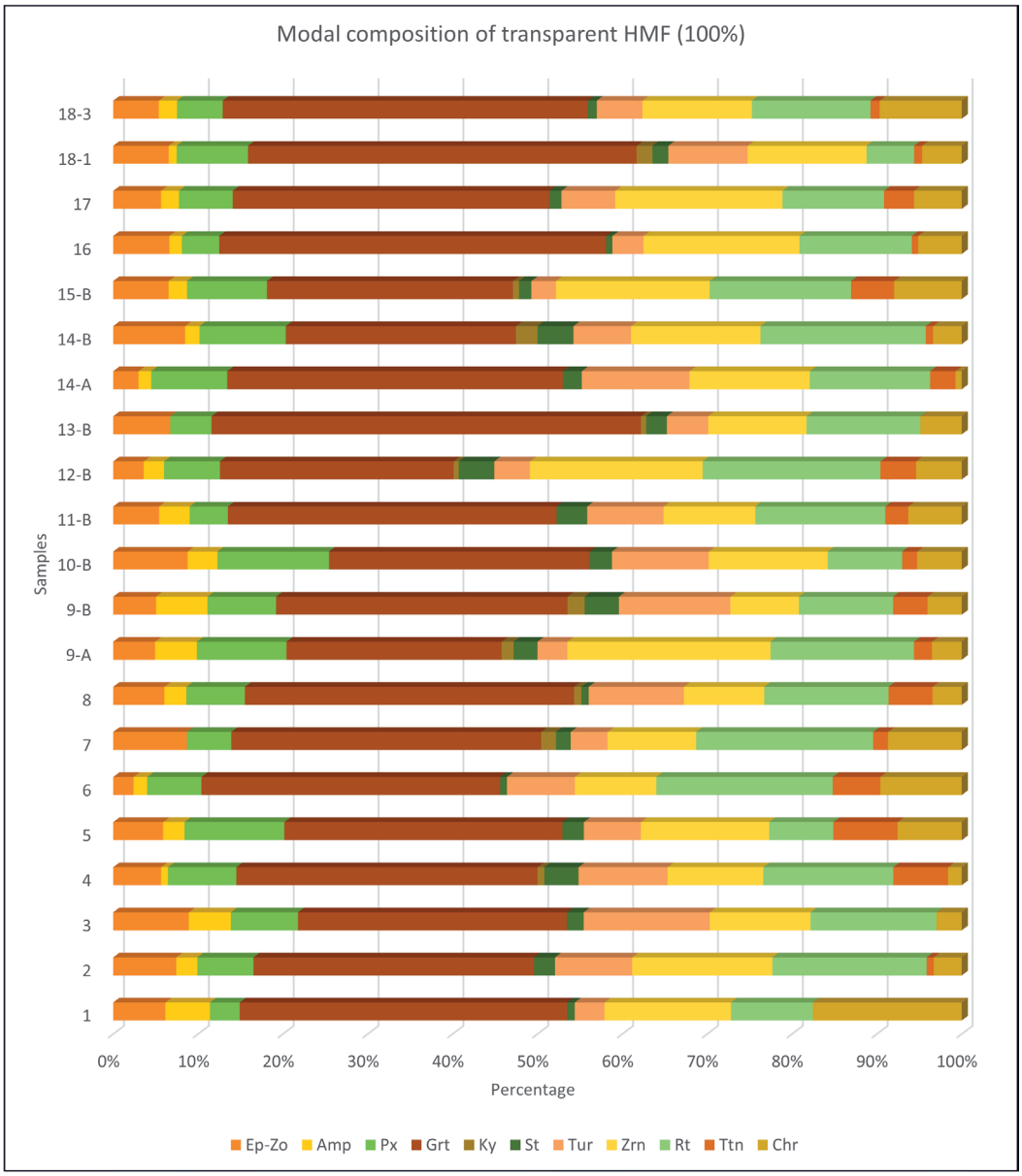

Figure 8. Modal composition of the TMF (values in %) (Legend in Table 5).

boles are represented by hornblende, and the pleochroic colours are dark green and olive green. It may be entirely fresh (Fig. 6o) or chloritized with black inclusions (probably magnetite) as an alteration product. Glaucophane is detected in the 14B horizon (Fig. 6p).

3.6. Petrographic analysis

Horizon 3 consists of angular to rounded carbonates (2/3 of the grains) and rounded dark chert pebbles (1/3 of the grains). Only one sample was determined as serpentinized olivine basalt (Fig. 9). The carbonates are of polygenetic origin, and they are formed in equal parts by strongly spherical, subrounded to rounded rudist limestones from the Upper Cretaceous and nummulitic limestones from the Eocene, as well as by low-spherical, angular to subangular carbonate concretions.

Based on the analysis of the rock fragments (Table 7), their composition, degree of roundness, and sorting, it can be concluded that the material has passed through several sedimentation cycles. The fragments are rounded to a considerable extent, the material was derived mainly from carbonate areas formed in different sedimentary environments, predominantly in shallow water areas, but also with some fragments from deep water areas of the basin represented.

The well-rounded and sorted grains of the rock fragments sampled in sublayer 9A are documented in Figure 10 as a) *Biconcava bentori Hamaoui* and *Saint-Marc*, b) *Nezzazatidae*, c) *Cuneolina* sp., d) *Rotalia* sp., e) *Nezzazatidae*, f) A – *Lituolidae*, B – *Pseudonummoloculina*, g) *Heterohelix globulosa Ehrenberg*, h) C – *Calcisphaerulidae*, H – *Heterohelix*, i) *Miliolidae*, j) *Valvulinidae*, k) *Rotalia* sp. and l) *Rotalia* sp. The determined fossils indicate an Upper Cretaceous age.

The dark pebble grains contain a selection of calcareous spherules (*Calcisphaerulidae* and *Heterohelix globulosa Ehrenberg*), which represent a deep-sea micro-association characteristic of the pelagic environment. They most probably have a Turonian – Senonian age. In the limestone grains, a shallow-water association consists mainly of benthic foraminifera (*Miliolidae, Textulariidae, Valvulinidae, Biconcava bentori*

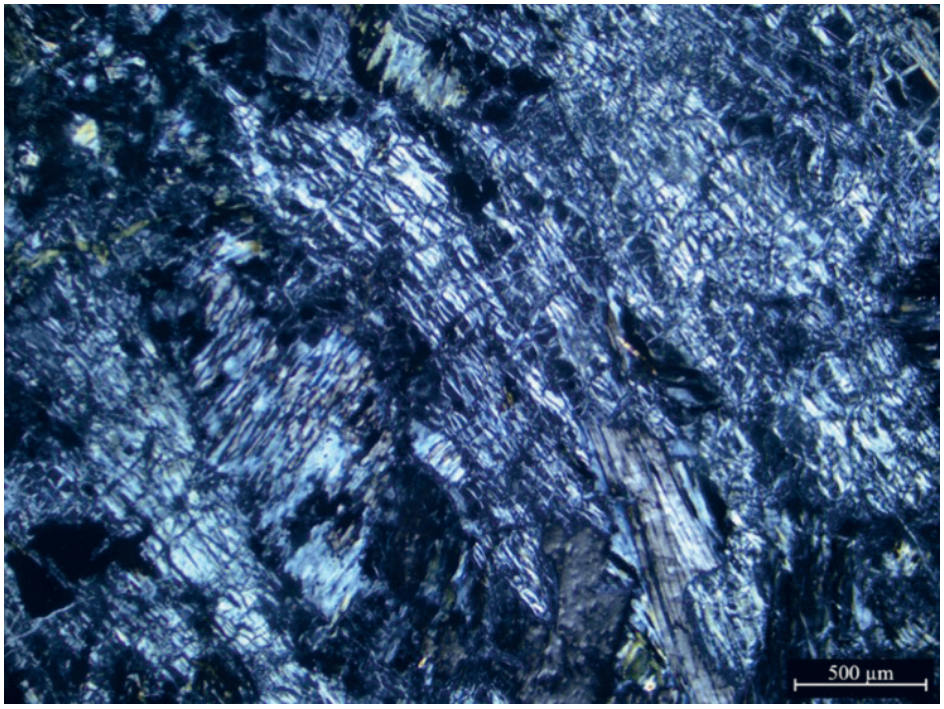

Figure 9. Photo-micrograph of serpentinized olivine basalt with crossed (N+) nicols.

Table 7. Percentage of rock fragments in a certain fraction of paleosol horizon 3.

Type of rocks	2-1.25 mm	2-0.9 mm	2- 0.5mm	<1.25mm	<0.9mm	0.5-0.06mm
	%					
Micritic limestone	19.77	31.14	43.27	17.42	16.67	30.15
Microsparitic limestone	63.95	56.28	40.71	71.61	68.23	19.14
Sparitic limestone	8,14	5.39	6.41	3.87	9.38	9.55
Siliciclastic rocks	5.81	7.19	8.33	5.16*	2.08*	39.31**
Bioclastic	2.33	-	1.28		2.08	1.12
Rock fragments (Fe rocks)	-	-		1.94	1.56	0.73
Σ	100	100	100	100	100	100

Legend: *chert; **chert, quarzite, quartz

Table 8. Depth, water content (W.C.), activity concentrations (Bq/kg) and dose rate (Gy/ka) estimate.

Sample	Horizon	Depth (cm)	W.C. (%)	Th-232 (Bq/kg)	U-238 (Bq/kg)	U-235 (Bq/kg)	K-40 (Bq/kg)	Dose rate (Gy/ka)
PN5-7	18	464	10 ± 5	7.7 ± 0.4	15 ± 3	0.69 ± 0.12	51 ± 3	0.70 ± 0.04
PN5-6	17	513	10 ± 5	13.7 ± 0.7	16 ± 4	0.74 ± 0.19	105 ± 6	0.96 ± 0.06
PN5-5	14B	604	10 ± 5	15.2 ± 0.7	13 ± 3	0.60 ± 0.14	80 ± 4	0.85 ± 0.05
PN5-4	13B	634	10 ± 5	18.9 ± 0.9	16 ± 4	0.74 ± 0.19	115 ± 6	1.05 ± 0.03
PN5-3	9B	718	10 ± 5	16.5 ± 1.0	13 ± 5	0.30 ± 0.15	85 ± 6	0.86 ± 0.06

Hamaoui and *Saint-Marc, Cuneolina* sp., *Lituolidae, Miliolidae, Nezzazatidae, Pseudonummoloculina*, *Quinqueloculina* sp.) and bryozoans. The age of these grains is probably also in the Upper Cretaceous (representing the Cenomanian to Lower Senonian, based on particular microfossils).

3.7. OSL dating

The results of the OSL dating of the upper GF complex are shown in Tables 8 and 9 as well as in Figure 11. The dose rate values are rather low, which can be explained by the relatively high quartz content of the samples. The relative standard deviation (RSD) of the measured dose populations is relatively large compared to the RSD of the dose determining test result (i.e. 5%), ranging between 21 – 31%. Since it is assumed that the site was saturated for a period and then very dry conditions prevailed in an indurated sediment mass, it can be assumed that bioturbation would have been a difficult process, causing mixing of the sediment and responsible for the observed overdispersion. However, given the glacio-fluvial nature of the sediment, insufficient bleaching of the quartz grains prior to deposition could be a problem. Therefore, we examined the dose populations towards smaller doses and attempted to

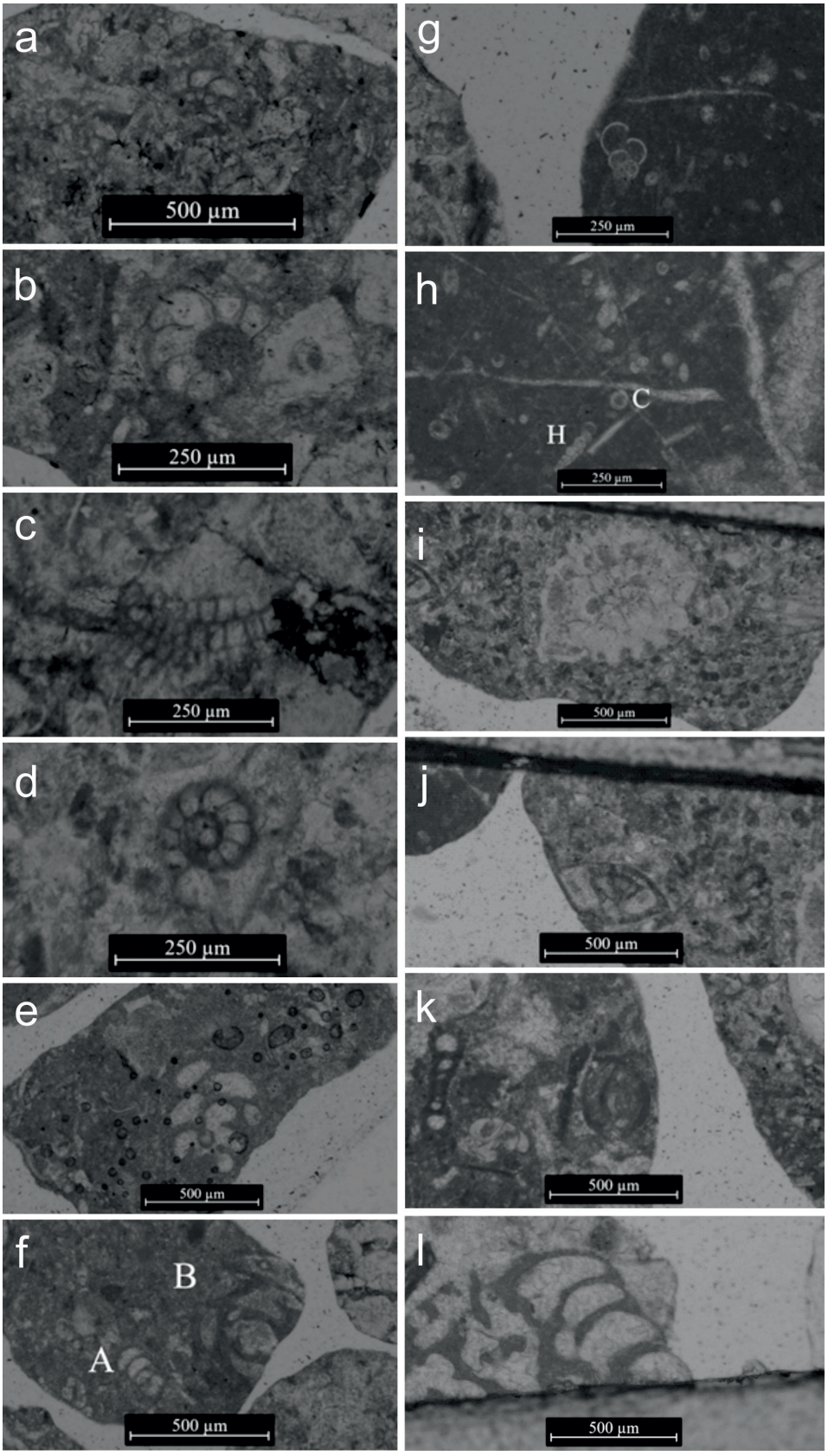

Figure 10. Photo-micrographs of course-sized sand grains from the 9A horizon: **a** *Biconcava bentori Hamaoui and Saint-Marc*; **b** *Nezzazatidae*; **c** *Cuneolina sp.*; **d** *Rotalia sp.*; **e** *Nezzazatidae*; **f** A – *Lituolidae*; B – *Pseudonummoloculina*; **g** *Heterohelix globulosa Ehrenberg*; **h** C – *Calcisphaerulidae*; H – *Heterohelix*; **i** *Miliolidae*; **j** *Valvulinidae*; **k** *Rotalia sp*; **l** *Rotalia sp.*

establish an apparent minimum age for the OSL samples. The minimum age is calculated using the "bottom 5%" method (i.e., in this case, an age derived from the aliquots with the two lowest dose values) from OLLEY et al. (1998) and is compared with the arithmetic mean. The latter is intended to be representative for the maximum age, given the fact that at least

Table 9. Number of aliquots that passed the rejection criteria, the relative standard deviation (RSD, %) of that population, and equivalent doses (De; Gy) and apparent ages (ka) based on the arithmetic mean and the lower 5% of the De population.

Sample	No. aliq.	RSD (%)	Arithmetic mean		Lower 5%	
			De (Gy)	Age (ka)	De (Gy)	Age (ka)
PN5-7	24	31	135 ± 9	193 ± 17	74 ± 9	105 ± 15
PN5-6	23	24	180 ± 8	188 ± 15	101 ± 7	105 ± 10
PN5-5	24	28	185 ± 6	218 ± 15	76 ± 5	90 ± 8
PN5-4	24	22	196 ± 6	186 ± 13	122 ± 7	116 ± 10
PN5-3	22	21	198 ± 7	229 ± 18	110 ± 15	128 ± 20

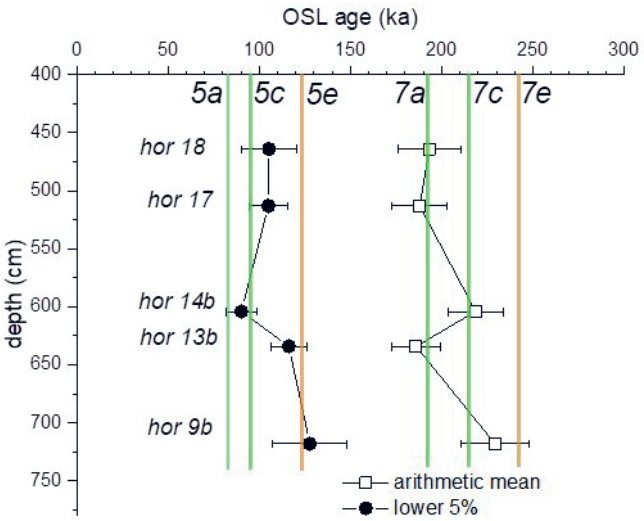

Figure 11. Age-depth plot showing the lower 5% results as a minimum estimate, and the arithmetic mean as a maximum estimate, with indication of sampling position (horizon number). Peak positions of significant interglacials (5e and 7e) and interstadials (5a, 5c, 7c and 7e) are indicated by vertical lines (COHEN & GIBBARD, 2019).

some aliquots would contain a certain proportion of insufficiently bleached grains. Of course, a significant proportion of the overdispersion is due to the heterogeneity in the beta dose rate. To summarize, the apparent OSL ages of the GF sediment overlying the palaeosol range are between ca. 230 ka and 130 ka for the lowermost sample and ca. 190 ka and 105 ka for the uppermost sample. Within the error limits, this means that the GF sediment in the minimum age scenario could have been deposited in the early Weichselian ice sheet and the palaeosol would have a later Eemian (MIS 5e) or older age (COHEN & GIBBARD, 2019). In the maximum age scenario, the glacio-fluvial sediment could even have an age roughly corresponding to the second half of the Saale Ice Age, which in turn means that the palaeosol could be as old as MIS 7e or even older.

4. DISCUSSION

The pedo-sedimentary succession of Privlaka is located in the central area of the Croatian part of the Adriatic coast. The investigated section is represented by an almost 2.70 m thick palaeosol complex on which a more than 5 m thick package of glacio-fluvial sediments was deposited.

The first ideas about Palaeoglaciation of Velebit Mt., (the most extensive mountain range of the Karst Dinarides) in Croatia, were developed at the beginning of the 20th century (ŽEBRE et al., 2021). The reconstructed ice cap area extended along the coastal mountains from Risnjak Mt. to south Velebit Mt. and across the range from Lika Polje to Rab Island (MARJANAC & MARJANAC, 2016). Investigating the glacial history of Velebit mountain, MARJANAC & MARJANAC (2004) described glacio-fluvial Late Pleistocene sands and gravels at an altitude of 900 m a.s.l., and glacio-lacustrine deposits (dominantly varved-like siltstones with dropstones) detected at sea level and below. They also detected those sediments on the opposite side of the Velebit channel, at Ražanac, as a probable time equivalent of those of the Novigradsko More section. VELIĆ et al. (2011) describe glacio-fluvial sediments in detail. They are composed of material redeposited from the till. Generally, glacio-fluvial deposits are composed of subrounded clasts and pebbles, which are smaller and better sorted than those found in till. They were formed by erosion of glacial deposits, in which erosional channels can be found on both sides of the terminal moraine (VELIĆ et al., 2011).

The pedo-sedimentary complex of Privlaka is divided into five (5) units. The lowest Unit I (thickness over 250 cm) shows the reddish palaeosol. This unit has vertically oriented carbonate concretions (rhizoconcretions) and carbonate nodules. The carbonate concretions in the base of the profile (Fig. 2b) are most probably developed in situ through impregnation related to groundwater or sea level fluctuations, and the remaining carbonate accumulations in the profile originated from predominantly carbonate glacio-fluvial material and aeolian sediments (Units II, III, IV and REC) (Fig. 2). Meteoric water enabled the dissolution, transport and precipitation of $CaCO_3$ in different forms, as described by GALOVIĆ (2016).

There are isolated magmatic pebbles associated with materials from the Dinaric ophiolitic zone in the hinterland. The boundary to the upper Unit II is characterized by wedges, which can be interpreted as desiccation cracks or possibly even frost cracks. Unit II, the (glacio-) fluvial material, consists of approximately 10 cm thick cyclic units (total thickness 120 cm) with grain-size fining upward. This unit contains predominantly of spherical carbonate concretions and lenticular structures filled with gravel. Subsequently, the material of Unit III shows a relative trend of fining upward, with clear gravel intercalations. As in Unit II, hemispherical to spherical carbonate concretions can be observed. In the upper part of this unit, subvertical root channels with carbonate coatings and subvertically oriented concretions (rhizoconcretions) occurred. Unit IV consists of glacio-fluvial material with a total thickness of 150 cm. There are cyclic events in which the grain size fines upward. The long-distance transport of the glacio-fluvial material of Units II, III and IV is confirmed by the presence of subrounded to rounded limestones.

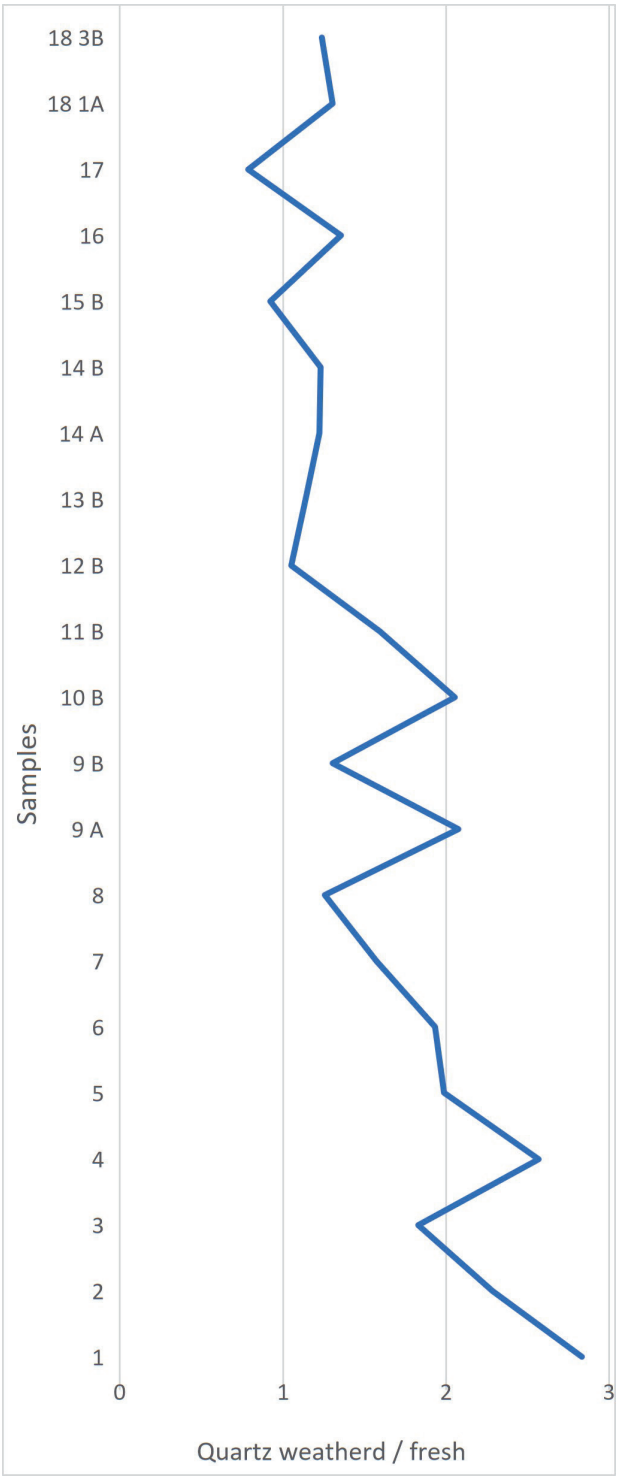

Figure 12. Distribution of the ratio of weathered and fresh quartz grains along the PN1-5 profile.

In Unit I, the increase in $CaCO_3$ content can partly be attributed to secondary carbonates (also observed in the field) precipitated as cement in carbonate concretions and rhizoconcretions in the lower part of profile PN1-5. PFAFFNER et al. (2024) in their investigations of loess – palaeosol sequences found various forms and sizes of secondary carbonate accumulation, i.e. pseudomycelia, hard nodules and soft carbonate concentrations.

From the physico-chemical properties, it can be concluded that the higher $CaCO_3$ content of Unit II (sub-layer 9A to 13B) is due to the increasing supply of the local lithogenic carbonate component (limestone fragments of sandy and silty grain size).

According to the pH results, all the analysed samples are alkaline pH_{H2O} (>7.5). In horizons with higher pH values (Fig. 4), carbonates can be found more frequently. DURN et al. (2018a) determined similar pH values in red palaeosols formed on the northern Adriatic island of Susak. These soils were also enriched with carbonate concretions. The organic matter content is higher in the palaeosol part of the pedo-sedimentary complex, which can be attributed to the pedogenetic processes in the lower part of the studied profile.

The grain-size analyses show that the sand fraction dominates in the glacio-fluvial (GF) sediments, while silt predominates in the palaeosol (PS) (Fig. 3). The upper part (GF) of the PN1-5 profile consists of fine or medium sands with several fining-upward sequences. The horizons of the palaeosol are classified as medium to coarse silts (WENTWORTH, 1922). Clay content is higher in the palaeosol, where pedogenetic processes were most intense. Both roundness (ranging between 0.14 and 0.62) and sphericity (ranging between 0.14 and 0.68) show a decreasing trend with smaller grain sizes in most of the individual samples. BANAK et al. (2021) found similar roundness characteristics for quartz grains in their investigations on the Adriatic coast. The authors concluded that the sand-gravel body is the result of sediment transport and deposition as part of a fluvial mechanism.

The modal composition of the analyzed samples, as well as the freshness and morphology of the individual mineral grains, indicate the different origins of the grains. The analyzed total fraction of the 0.09 – 0.125 mm quartz grains in the LMF accounts for about 85% of the non-carbonate minerals (Tables 5 and 6). Comparing this with the proportion of quartz grains in the loess of continental Croatia (GALOVIĆ, 2016; GALOVIĆ & PEH, 2016), where quartz is also dominant but represented by only 50 – 75% of the LMF, it can be assumed that these sediments have undergone more redeposition than the grains of a typical continental loess. A similar proportion of quartz in the LMF is also present in the loess of the northern Adriatic island of Susak (50 – 60%) (MIKULČIĆ PAVLAKOVIĆ et al., 2011). Therefore, when FAIVRE et al. (2019) examined fluvial sediments on the coast of the island of Vis (central Adriatic), they found that in most samples around 60% of the quartz grains were weathered. These samples contained more feldspars than in the present study, so they were also able to determine the proportions of fresh and weathered feldspars. Weathered feldspar grains dominated 1.5 to 6.5 times. In Privlaka, there is a general trend of an increase in the proportion of weathered quartz grains with depth (Fig. 12). The ratio is about 1:1 in the upper part of PN1-5 profile (layer 12 and above) and reaches, with fluctuations, almost 3:1 in the lowest horizon. This could indicate that the proportion of fluvial sediments increases with depth compared to aeolian sediments.

Weathered quartz grains often have a regeneration rim that indicates several recrystallization sequences (Fig. 6a3). In addition, weathered quartz and feldspar grains have no visible inclusions (Figs. 6a2–3, b), whereas fresh grains are idiomorphic or hypidiomorphic and contain inclusions (Figs. 6a–c). Idiomorphic and hypidiomorphic grains, especially feldspars,

which are not resistant to chemical weathering, and accessory volcanic glass form part of the aeolian contribution (DURN et al., 1999, 2018b). This assumption is also supported by the presence of quartz spherules formed by devitrification (Fig. 6f), as well as the freshness of some grains, otherwise weatherable zircons (Fig. 6l) and amphiboles such as hornblende and glaucophane (Figs. 6o, p). If we focus on the dominant minerals of the THM, represented by resistant minerals such as garnet, zircon and tourmaline, the polygenetic origin of the material is confirmed by the presence of fresh idiomorphic grains with inclusions (Figs. 6i, k) and allotriomorphic rounded grains without inclusions (Figs. 7h, j).

A comparison of the modal compositions of the Privlaka pedosediment complex with the loess sections (mainly of Alpine origin) of the island of Susak (MIKULČIĆ PAVLAKOVIĆ et al., 2011) shows a significant difference in spinel content. The Susak loess is resedimented fluvial material from the Po basin, and chromite is an accessory or absent component of the HMF (MIKULČIĆ PAVLAKOVIĆ et al., 2011). However, up to 18% chromite in the THM of the Privlaka section indicates a significant intake of material from sources other than the Po Plain. In addition to the dominant Cr-rich reddish chromite, yellowish-brown Cr-rich picotite? was also found, which is characteristic of basic and ultrabasic rocks and is associated with volcanic rocks, peridotites and serpentinites (Fig. 6n). Chromite, serpentinite (Figs. 6m, n, g, 10; Table 6) and serpentinized olivine basalt (Fig. 9) indicate an area of origin with ultramafic rocks. WACHA et al. (2019) found similar mineral phases in their study. The authors concluded that chromite grains indicate an ultramafic rock source, most likely the rocks from the Inner Dinarides. The presence of chert (Fig. 5; Table 5) and siliceous fossils (siliceous spicules of fossil sponges (Fig. 6d) and fossil zonal chert spherules (Fig. 6e) is the starting point for the palaeontological approach to trace the area of origin. In addition, mineralogical analysis confirmed chromium hydroxides in the palaeosol, indicating the weathering of chromium-bearing rocks such as peridotites and similar ultrabasic rocks and their alteration products (serpentinites) (SCHINDLER & MCLENAGHAN, 2022). Petrographic and modal analysis revealed that some pebbles and particles in the palaeosol represent ultramafic rocks. The chromium hydroxides are probably the product of the weathering of these rock fragments.

Cretaceous and Eocene limestones dominate the pre-Quaternary rocks in the study area (MAJCEN & KOROLIJA, 1973; ILIJANIĆ et al., 2018), while Eocene conglomerates, rich in spherical, rounded, dark chert pebbles, occur sporadically in outcrops in the source area. Chert is almost 1000 times harder than carbonate. Since the shape of the chert pebbles was the same in the source area (MAJCEN & KOROLIJA, 1973), it cannot be used as an indicator of the intensity and distance of transportation. However, subrounded and rounded limestone fragments of the same age indicate long, intensive transport, probably with several resedimentation episodes. In contrast, angular and subangular carbonate concretions indicate a local origin and shorter transport. As such, carbonate concretions are a product of translocation and precipitation of carbonates during pedogenesis, it could be concluded that these concretions were precipitated at the bottom of that pedological profile during palaeopedogenesis (POCH et al., 2024; HUSNJAK et al., 2025), which occurred prior to sedimentation of the parent material of horizon 3.

The erosion of this older palaeosol exposed these concretions, so that they were also exposed to further erosion. It can be assumed that the concretions were transported by the same mechanism as the already eroded older palaeosol and that both materials were resedimented at the investigated site. At this point, these sediments became the parent material for the new pedogenesis of horizon 3. There is a high probability that this parent material, which contained carbonate concretions formed during an older pedogenesis, also contained soil material from the same older palaeosol that was eroded and brought together by glacio-fluvial transport. This mechanism is described in the examples of resedimented palaeosols in continental (GALOVIĆ, 2014, 2016; GALOVIĆ et al., 2023, 2024; POCH et al., 2024) and Mediterranean Croatia (FAIVRE et al., 2019; HUSNJAK et al., 2025; POCH et al., 2024). Therefore, we cannot assume that the degree of pedogenetic development of the studied palaeosol horizon 3 reflects the climatic conditions that prevailed during its pedogenesis. Indeed, the bottom sediment was exposed to pedogenesis and was deposited together with other eroded sediments. In contrast, it is merely the erosion product of a landscape from which the weathered topsoil was removed and redeposited in the studied section.

Based on the OSL dating results, the red palaeosol in the lower part of the pedo-sedimentary complex could be as old as MIS 5e (Eemian) or even older. A similar age for the red palaeosol was found by DURN et al. (2018a) in their study. Although the OSL dating results clearly demonstrate the old age of succession, we do not recommend proposing exact age estimates from it for two reasons. Firstly, given the sedimentary environment of the quartz used for dating, insufficient bleaching of some or a significant proportion of the grains cannot be ruled out and may even be plausible. For this reason, we consider it safe to determine only a minimum age based on the "lower 5%" approach. Secondly, the equivalent doses determined are in the high dose range for quartz (i.e., approximately between 70 – 200 Gy), which could be questionable regarding the reliability of the method (obvious underestimation of age). However, it should be noted that such effects are often only observed at equivalent doses of more than 200 Gy (ANACHITEI-DEACU et al., 2018). Independent methods such as cosmogenic radionuclide dating could help to further constrain the age model for the Privlaka succession.

4. CONCLUSION

This study contains mineralogical and sedimentological results and the first description of the Quaternary succession of palaeosol and sediments in Privlaka (eastern Adriatic coast, Croatia). The investigated sediments form a vertical, 8 m thick succession of glacio-fluvial (GF) sand resting on an underlying silty (PS) palaeosol.

According to the OSL dating results, the glacio-fluvial sand is either early Weichselian or Saalian in age, while the palaeosol most likely cannot be younger than the Eemian and could even have a Middle Pleistocene age.

The higher $CaCO_3$ content in the upper part of the pedosedimentary succession of Privlaka (GF; Units II, III and IV; sub-layers 9A to 18-3) can be attributed to the increase in the supply of the local lithogenic carbonate component (limestone fragments of sandy and silty grain size), whereas in the lower part the increase in $CaCO_3$ content is partially due to the precipitation of secondary carbonates (which was also observed in the field).

The results of the modal analysis show up to 18% chromite in the THM of the Privlaka section, indicating a significant input of material from sources other than the Po Plain. In addition to the predominant Cr-rich reddish chromite, yellowish-brown Cr-rich picotite was also detected, which is characteristic of basic and ultrabasic rocks associated with volcanic rocks, peridotites, and serpentinites. In addition, the mineralogical analysis confirmed chromium hydroxides in the palaeosol, indicating the weathering of chromium-rich rocks such as peridotites and similar ultrabasic rocks and their transformation products (serpentinites). All the rocks and accompanying minerals mentioned indicate an area of origin with ultramafic rocks from the Dinaric ophiolitic zone in the hinterland.

Subrounded and rounded limestone fragments of the same age indicate long, intensive glacio-fluvial transport, probably with several resedimentation episodes. However, angular and subangular carbonate concretions indicate a local origin. Since such carbonate concretions are a product of translocation and precipitation of carbonates during pedogenesis, one could conclude that these concretions were precipitated at the bottom of that pedological profile during paleopedogenesis.

ACKNOWLEDGEMENT

This research is funded by the Croatian Science Foundation under the project ACCENT (IP-2020-02-3274). We are grateful to the associate editor and the reviewers for their thorough evaluations, which significantly improved the manuscript.

REFERENCES

ADAMIEC, G. & AITKEN, M. (1998): Dose-rate conversion factors: update.– Ancient TL 16, 37-50.

ANECHITEI-DEACU, V., TIMAR-GABOR, A., THOMSEN, K.J., BUYLAERT, J.-P., JAIN, M., BAILEY, M. & MURRAY, A.S. (2018): Single and multi-grain OSL investigations in the high dose range using coarse quartz.– Radiation Measurements, 120, 124–130. https://doi.org/10.1016/j.radmeas.2018.06.008

BANAK, A., PAVELIĆ, D., KOVAČIĆ, M. & MANDIĆ, O. (2013): Sedimentary characteristics and source of loess in Baranja (Eastern Croatia).– Aeolian Research, 11, 129–139. https://doi.org/10.1016/j.aeolia.2013.08.002

BANAK, A., PIKELJ, K., LUŽAR-OBERITER, B. & KORDIĆ, B. (2021): The sedimentary record of Pleistocene aeolian–alluvial deposits on Vrgada Island (eastern Adriatic coast, Croatia).– Geologia Croatica, 74/2, 127–137. https://doi.org/10.4154/gc.2021.14

BEERTEN, K., VERBEECK, K., LALOY, E., VANACKER, V., VANDENBERGHE, D., CHRISTL, M., DE GRAVE, J. & WOUTERS, L. (2020): Electron spin resonance (ESR), optically stimulated luminescence (OSL) and terrestrial cosmogenic radionuclide (TCN) dating of quartz from a Plio-Pleistocene sandy formation in the Campine area, NE Belgium.– Quaternary International, 556, 144–158. https://doi.org/10.1016/j.quaint.2020.06.011

BEERTEN, K., GALOVIĆ, L., PANDUROV, M., STEJIĆ, P., GAJIĆ, R., HEĆEJ, N., MARTINČEVIĆ LAZAR, J., KORDIĆ, B. & PJANIĆ, A. (2025): Characteristics of Late Pleistocene and Holocene dune activity and soil formation in the Podravina, NE Croatia.– Quaternary Research, 1–19. https://doi.org/10.1017/qua.2025.10023

BEHR LABOR-TECHNIK (2017): SCM1 Calcimeter for determination of the carbonate content of a soil sample. User's Manual.– BEHR Labor-Technik GmbH, Düsseldorf, 15 p.

BREWER, R. (1976): Fabric and Mineral Analysis of Soils.– Krieger, Huntington, New York, 482 p.

COHEN, K.M. & GIBBARD, P. (2019): Global chronostratigraphical correlation table for the last 2.7 million years, version 2019. QI-500.– Quaternary International, 500, 20–31. https://doi.org/10.1016/j.quaint.2019.03.009

CORREGGIARI, A., ROVERI, M. & TRINCARDI, F. (1996): Late Pleistocene and Holocene Evolution of the North Adriatic Sea.– Quaternario, 9/2, 697–704.

DURN, G. (1996): Origin, composition and genesis of terra rossa in Istria [in Croatian].– Unpubl. PhD Thesis, University of Zagreb, 204 p.

DURN, G., OTTNER, F. & SLOVENEC, D. (1999): Mineralogical and geochemical indicators of the polygenetic nature of terra rossa in Istria, Croatia.– Geoderma, 91, 125–150. https://doi.org/10.1016/S0016-7061(98)00130-X

DURN, G., WACHA, L., BARTOLIN, M., ROLF, C., FRECHEN, M., TSUKAMOTO, S., TADEJ, N., HUSNJAK, S., LI, Y. & RUBINIĆ, V. (2018a): Provenance and formation of the red paleosol and lithified terra rossa-like infillings on the Island of Susak: A high-resolution and chronological approach.– Quaternary International, 494, 105–129. https://doi.org/10.1016/j.quaint.2017.11.040

DURN, G., RUBINIĆ, V., WACHA, L., PATEKAR, M., FRECHEN, M., TSUKAMOTO, S., TADEJ, N. & HUSNJAK, S. (2018b): Polygenetic soil formation on Late Glacial Loess on the Susak Island reflects paleo-environmental changes in the Northern Adriatic area.– Quaternary International, 494, 236–247. https://doi.org/10.1016/j.quaint.2017.06.072

DURN, G., PERKOVIĆ, I., STUMMEYER, J., OTTNER, F. & MILEUSNIĆ, M. (2021): Differences in the behaviour of trace and rare-earth elements in oxidizing and reducing soil environments: Case study of Terra Rossa soils and Cretaceous paleosols from the Istrian peninsula, Croatia.– Chemosphere, 283, 131286. https://doi.org/10.1016/j.chemosphere.2021.131286

FAIVRE, S., GALOVIĆ, L., SÜMEGI, P., CVITANOVIĆ, M., NÁFRÁDI, K. & HORVATINČIĆ, N. (2019): Palaeoenvironmental reconstruction of the Milna valley on the island of Vis (Central Adriatic) during the late Holocene.– Quaternary International, 510, 1–17. https://doi.org/10.1016/j.quaint.2018.11.017

GALOVIĆ, L. (2014): Geochemical archive in the three loess/paleosol sections in the Eastern Croatia: Zmajevac I, Zmajevac and Erdut.– Aeolian Research, 15, 113–132. https://doi.org/10.1016/j.aeolia.2014.07.004

GALOVIĆ, L. (2016): Sedimentological and mineralogical characteristics of the Pleistocene loess/paleosol sections in the Eastern Croatia.– Aeolian Research, 20, 7–23. https://doi.org/10.1016/j.aeolia.2015.10.007

GALOVIĆ, L. & PEH, Z. (2016): Mineralogical discrimination of the Pleistocene loess/paleosol sections in Srijem and Baranja, Croatia.– Aeolian Research, 21, 151–162. doi:10.1016/j.aeolia.2016.04.006

GALOVIĆ, L., FRECHEN, M., PEH, Z., DURN, G. & HALAMIĆ, J. (2011): Loess/palaeosol section in Šarengrad, Croatia – a qualitative discussion on the correlation of the geochemical and magnetic susceptibility data.– Quaternary International, 240, 1–2, 22–34. https://doi.org/10.1016/j.quaint.2011.02.003

GALOVIĆ, L., HUSNJAK, S., ŠORŠA, A. & MARTINČEVIĆ LAZAR, J. (2023): Evidence and mineralogical and physico-chemical properties of chernozem and chernozem-like soils in Croatia.– Geologia Croatica, 76/3, 113–129. https://doi.org/10.4154/gc.2023.08

GALOVIĆ, L., ŠORŠA, A. & PEH, Z. (2024): Modelling the paleopedological development of loess/palaeosol sections using discriminant function analysis of compositional geoscience data, case study in Eastern Croatia.– Journal of Geochemical Exploration, 262, 107473. https://doi.org/10.1016/j.gexplo.2024.107473

HRN ISO 10390 (2005): Soil quality – Determination of pH (ISO 10390:2005).– Croatian Standard Institute, Zagreb.

HUSNJAK, S., GALOVIĆ, L., POCH, R.M., MARTINČEVIĆ LAZAR, J. & PJANIĆ, A. (2025): Influences of fluvial and aeolian processes on palae-

osols formation in Privlaka, Croatia.– Geoderma Regional, 40, e00942. https://doi.org/10.1016/j.geodrs.2025.e00942

ILIJANIĆ, N., MIKO, S., HASAN, O. & BAKRAČ, K. (2018): Holocene environmental record from lake sediments in the Bokanjačko blato karst polje (Dalmatia, Croatia).– Quaternary International, 494, 66–79. https://doi.org/10.1016/j.quaint.2018.01.037

KRUMBEIN, W. & SLOSS, L. (1963): Stratigraphy and Sedimentation.– W.H. Freeman and Co., San Francisco, 660 p.

MAJCEN, Ž. & KOROLIJA, B. (1973): Osnovna geološka karta SFRJ 1:100 000. Tumač za list Zadar [*Basic Geological Map of SFRY 1:100 000, Zadar sheet* – in Croatian].– Institut za geološka istraživanja, Zagreb, Savezni geološki zavod, Beograd.

MAJCEN, Ž., KOROLIJA, B., SOKAČ, B. & NIKLER, L. (1970): Osnovna geološka karta SFRJ 1:100 000, list Zadar [*Basic Geological Map of SFRY 1:100 000, Zadar sheet* – in Croatian].– Institut za geološka istraživanja, Zagreb, Savezni geološki zavod, Beograd.

MARJANAC, LJ. & MARJANAC, T. (2004): Glacial history of the Croatian Adriatic and coastal Dinarides.– In: EHLERS J. & GIBBARD PL. (eds): Developments in quaternary sciences.– Part I: Europe. Elsevier, Amsterdam, 19–26. https://doi.org/10.1016/S1571-0866(04)80053-8

MARJANAC, T. & MARJANAC, LJ. (2016): The extent of middle Pleistocene ice cap in the coastal Dinaric Mountains of Croatia.– Quaternary Research, 85/3, 445–455. https://doi.org/10.1016/j.yqres.2016.03.006

MIKULČIĆ PAVLAKOVIĆ, S., CRNJAKOVIĆ, M., TIBLJAŠ, D., ŠOUFEK, M., WACHA, L., FRECHEN, M. & LACKOVIĆ, D. (2011): Mineralogical and geochemical characteristics of quaternary sediments from the island of Susak (Northern Adriatic, Croatia).– Quaternary International, 234, 32–49. https://doi.org/10.1016/j.quaint.2010.02.005

MOLNÁR, D., MAKÓ, L., CSEH, P., SÜMEGI, P., FEKETE, I. & GALOVIĆ, L. (2021): Middle and Late Pleistocene Loess-Paleosol Archives in East Croatia: Multi-proxy Palaeoecological Studies on Zmajevac and Šarengrad II Sequences.– Studia Quaternaria, 38/1, 3–17. https://doi.org/10.24425/sq.2020.133758

MUNSELL SOIL COLOUR CHARTS (2013): Munsell Soil Color Charts with genuine Munsell color chips.– Macbeth Division of Kollmorgem Instruments Corporation, New Windsor.

MURRAY, A.S. & WINTLE, A.G. (2003): The single aliquot regenerative dose protocol: potential for improvements in reliability.– Radiation Measurements, 37, 377–381. https://doi.org/10.1016/S1350-4487(03)00053-2

OLLEY, J.M., CAITCHEON, G. & MURRAY, A.S. (1998): The distribution of apparent dose as determined by optically stimulated luminescence in small aliquots of fluvial quartz: implications for dating young sediments.– Quaternary Science Reviews, 17, 1033–1040. https://doi.org/10.1016/S0277-3791(97)00090-5

PDF-4/MINERALS (2024): MDI Materials Data.– Livermore, CA, USA.

PFAFFNER, N., KADEREIT, A., KARIUS, V., KOLB, T., KREUTZER, S. & SAUER, D. (2024): Reconstructing the Eemian to Middle Pleniglacial pedosedimentary evolution of the Baix loess–palaeosol sequence (Rhône Rift Valley, southern France) – basic chronostratigraphic framework and palaeosol characterization.– E&G Quaternary Science Journal, 73, 1–22. https://doi.org/10.5194/egqsj-73-1-2024

POCH, R.M., GALOVIĆ, L., HUSNJAK, S., MARTINČEVIĆ LAZAR, J., HEĆEJ, N., RUŽIČIĆ, S., PJANIĆ, A., ÁLVAREZ, D., BEERTEN, K., GAJIĆ, R., STEJIĆ, P. & PANDUROV, M. (2024): Soil formation and environmental reconstruction of a loess-paleosol sequence in Zmajevac, Croatia.– Catena, 247, 108507. https://doi.org/10.1016/j.catena.2024.108507

PRESCOTT, J.R. & HUTTON, J.T. (1994): Cosmic ray contributions to dose rates for luminescence and ESR dating: large depths and long-term time variations.– Radiation Measurements, 23, 497–500. https://doi.org/10.1016/1350-4487(94)90086-8

RETALLACK, G.J. (2019): Soils of the Past: An Introduction to Paleopedology, 3rd Edition.– Blackwell Science Ltd., Oxford, 552 p. https://doi.org/10.1002/9780470698716

SCHINDLER, M. & MCLENAGHAN, N.W. (2022): Release of chromite nanoparticles and their alteration in the presence of Mn-oxides.– American Mineralogist, 107/4, 642–653. https://doi.org/10.2138/am-2021-7881

SHANG, C. & ZELAZNY, L.W. (2008): Selective Dissolution Techniques for Mineral Analysis of Soils and Sediments.– In: ULERY, A.L. & DREES, L.R. (eds.): Methods of Soil Analysis, Part 5 – Mineralogical Methods, SSSA Book Series, no. 5., Soil Science of America, 33–80. https://doi.org/10.2136/sssabookser5.5.c3

SIART, C., HECHT, S., HOLZHAUER, I., ALTHERR, R., MEYER, H., SCHUKRAFT, G., EITEL, B., BUBENZER, O. & PANAGIOTOPOULOS, D. (2010): Karst depressions as geoarchaeological archives: The palaeoenvironmental reconstruction of Zominthos (Central Crete), based on geophysical prospection, sedimentological investigations, and GIS.– Quaternary International, 216, 1–2, 75–92. https://doi.org/10.1016/j.quaint.2009.06.020

SPRAFKE, T., SCHULTE, P., MEYER-HEINTZE, S., HÄNDEL, M., EINWÖGERER, T., SIMON, U., PETICZKA, R., SCHÄFER, C., LEHMKUHL, F. & TERHORST, B. (2020): Paleoenvironments from robust loess stratigraphy using high-resolution color and grain-size data of the last glacial Krems-Wachtberg record (NE Austria).– Quaternary Science Reviews, 248, 106602. https://doi.org/10.1016/j.quascirev.2020.106602

ÚJVÁRI, G., KOK, J.F., VARGA, G. & KOVÁCS, J. (2016): The physics of wind-blown loess: Implications for grain size proxy interpretations in Quaternary paleoclimate studies.– Earth-Science Reviews, 154, 247–278. http://dx.doi.org/10.1016/j.earscirev.2016.01.006

VANDENBERGHE, D., DE CORTE, F., BUYLAERT, J.P., KUČERA, J. & VAN DEN HAUTE, P. (2008): On the internal radioactivity in quartz.– Radiation Measurements, 43, 771–775. https://doi.org/10.1016/j.radmeas.2008.01.016

VELIĆ, J., VELIĆ, I. & KLJAJO, D. (2011): Sedimentary bodies, forms and occurences in the Tudorevo and Mirovo glacial deposits of northern Velebit (Croatia).– Geologia Croatica, 64, 1–16.

WACHA, L. & FRECHEN, M. (2011): The geochronology of the „Gorjanović loess section" in Vukovar, Croatia.– Quaternary International, 240/1, 87-99. https://doi.org/10.1016/j.quaint.2011.04.010

WACHA, L., MIKULIĆ PAVLAKOVIĆ, S., FRECHEN, M. & CRNJAKOVIĆ, M. (2011): The Loess Chronology of the Island of Susak, Croatia.– E&G Quaternary Science Journal, 60/1, 153–169. https://doi.org/10.3285/eg.60.1.11

WACHA, L., MONTANARI, A., LOMAX, J., FIEBIG, M., LÜTHGENS, C., KORBAR, T. & KOEBERL, C. (2019): Last Glacial Maximum giant sand dunes on the island of Vis, Croatia.– In: KOEBERL, C. & BICE, D.M. (eds.): 250 Million Years of Earth History in Central Italy: Celebrating 25 Years of the Geological Observatory of Coldigioco: Geological Society of America Special Paper, 459–470, 542 p. https://doi.org/10.1130/2019.2542(26)

WARR, L.N. (2021): IMA–CNMNC approved mineral symbols.– Mineralogical Magazine, 85, 291–320. https://doi.org/10.1180/mgm.2021.43.

WENTWORTH, C.K. (1922): A scale of grade and class terms for clastic sediment.– Journal of Geology, 30, 377–392. https://doi.org/10.1086/622910

ZERBONI, A., TROMBINO, L., FRIGERIO, C., LIVIO, F., BERLUSCONI, A., MICHETTI, A.M., RODNIGHT, H. & SPÖTL, C. (2015): The loess-paleosol sequence at Monte Netto: A record of climate change in the Upper Pleistocene of the central Po Plain, northern Italy.– Journal of Soils and Sediments, 15, 1329–1350. https://doi.org/10.1007/s11368-014-0932-2

ŽEBRE, M., SARIKAYA, M.A., STEPIŠNIK, U., COLUCCI, R.R., YILDIRIM, C., ÇINER, A., CANDAŞ, A., VLAHOVIĆ, I., TOMLJENOVIĆ, B., MATOŠ, B. & WILCKEN, K.M. (2021): An early glacial maximum during the last glacial cycle on the northern Velebit Mt. (Croatia). Geomorphology, 392, 107918. https://doi.org/10.1016/j.geomorph.2021.107918

Web source:

GOOGLE MAPS (2025): Republic of Croatia. Accessed at: https://www.google.com/maps/place/Croatia/@44.23455,15.7881617,525170m/data=!3m1!1e3!4m6!3m5!1s0x133441080add95ed:0xa0f3c024e1661b7f!8m2!3d45.1!4d15.2000001!16zL20vMDFwajc?entry=ttu. Accessed on: February 15th, 2025.